AD-A206 099 FLOW-TURNING LOSSES IN SOLID ROCKET MOTORS(U) HERSH ACOUSTICAL ENGINEERING CHATSWORTH CA A S HERSH ET AL. 1/1
MAR 88 AFAL-TR-87-095 F04611-81-C-0041

UNCLASSIFIED F/G 21/8 2 NL

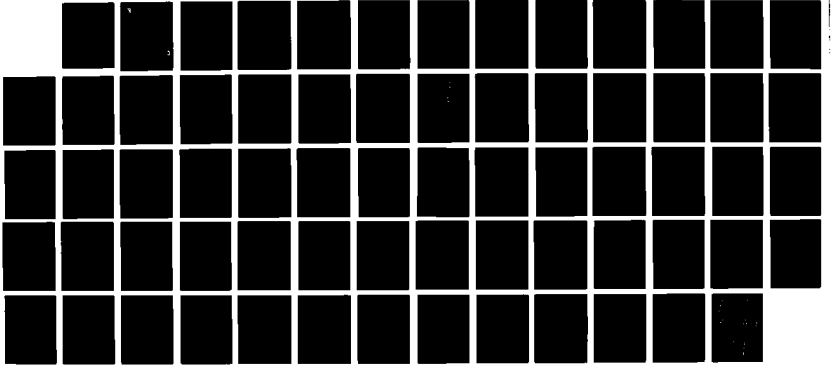

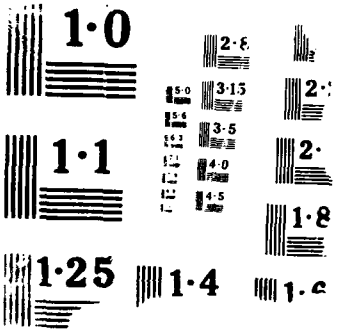
1·0
1·1
1·25
1·4
3·15
3·5
4·0
4·5
1·8

(2)

AFAL-TR-87-095

AD:

Final Report
for the period
July 1981 to
March 1988

Flow-Turning Losses in Solid Rocket Motors

March 1988

Authors:
A. S. Hersh
J. Tso

Hersh Acoustical Engineering, Inc.
9545 Cozycroft Ave.
Chatsworth, CA 91311

F04611-81-C-0041

Approved for Public Release

Air Force Astronautics Laboratory

Air Force Space Technology Center
Space Division, Air Force Systems Command
Edwards Air Force Base,
California 93523-5000

NOTICE

When U.S. Government drawings, specifications, or other data are used for any purpose other than a definitely related Government procurement operation, the fact that the Government may have formulated, furnished, or in any way supplied the said drawings, specifications, or other data, is not to be regarded by implication or otherwise, or in any way licensing the holder or any other person or corporation, or conveying any rights or permission to manufacture, use, or sell any patented invention that may be related thereto.

FOREWORD

This final report was submitted by Hersch Acoustical Engineering, Inc., Chatsworth, CA on completion of contract F04611-81-C-0041 with the Air Force Astronautics Laboratory (AFAL), Edwards AFB, CA. AFAL Project Manager was Gary Vogt.

This report has been reviewed and is approved for release and distribution in accordance with the distribution statement on the cover and on the DD Form 1473.

GARY L. VOGT
Project Manager

LAWRENCE P. QUINN
Chief, Aerothermochemistry Branch

FOR THE COMMANDER

HOMER M. PRESSLEY, Jr, Lt Col, USAF
Chief, Astronautical Sciences Division

SECURITY CLASSIFICATION OF THIS PAGE

REPORT DOCUMENTATION PAGE

Form Approved
OMB No. 0704-0188

1a REPORT SECURITY CLASSIFICATION Unclassified	1b RESTRICTIVE MARKINGS None
2a SECURITY CLASSIFICATION AUTHORITY	3 DISTRIBUTION/AVAILABILITY OF REPORT Approved for public release; distribution is unlimited.
2b DECLASSIFICATION/DOWNGRADING SCHEDULE	
4 PERFORMING ORGANIZATION REPORT NUMBER(S)	5 MONITORING ORGANIZATION REPORT NUMBER(S) AFAL-TR-87-095
6a NAME OF PERFORMING ORGANIZATION Hersh Acoustical Engineering, Inc. — 6b OFFICE SYMBOL (If applicable)	7a NAME OF MONITORING ORGANIZATION Air Force Astronautics Laboratory
6c ADDRESS (City, State, and ZIP Code) 9545 Cozycroft Avenue Chatsworth, Ca. 91311	7b ADDRESS (City, State, and ZIP Code) AFAL/DYC Edwards AFB, CA 93523-5000
8a NAME OF FUNDING/SPONSORING ORGANIZATION — 8b OFFICE SYMBOL (If applicable)	9 PROCUREMENT INSTRUMENT IDENTIFICATION NUMBER F04611-81-C-0041
8c ADDRESS (City, State, and ZIP Code)	10 SOURCE OF FUNDING NUMBERS

PROGRAM ELEMENT NO	PROJECT NO	TASK NO	WORK UNIT ACCESSION NO
62302F	5730	10	LP

11 TITLE (Include Security Classification)
Flow-Turning Losses in Solid Rocket Motors (U)

12 PERSONAL AUTHOR(S)
Alan S. Hersh and Jin Tso

13a TYPE OF REPORT	13b TIME COVERED	14 DATE OF REPORT (Year, Month, Day)	15 PAGE COUNT
Final	FROM 81/7 TO 88/3	88/3	66

16 SUPPLEMENTARY NOTATION

17 COSATI CODES		
FIELD	GROUP	SUB-GROUP
21	08	2
20	01	

18 SUBJECT TERMS (Continue on reverse if necessary and identify by block number)
Sound Absorption, Sound Attenuation, Sound/Flow Interaction, Sound/Flow Energy Exchange, Flow-Turning Acoustic Losses, Combustion Instability.

19 ABSTRACT (Continue on reverse if necessary and identify by block number)

Results are presented of an experimental and analytical investigation of the "flow-turning" losses resulting from the injection of ambient air into an acoustically energized duct. Measurements show that acoustic energy is absorbed. In all test cases, however, the sound energies absorbed by the finite admittance duct sidewalls were significantly larger than that absorbed by the injected flows.

One-dimensional steady-state and transient "flow-turning" solutions were derived. For the special case of rigid walls and low injection rates, the steady-state solutions showed that the "flow-turning" losses were approximately equal to 10 Log (1-Mav) where Mav is the average Mach number across the duct cross-section. The one-dimensional solutions inadequately predicted the measured acoustic energy losses.

The transient solutions compared very favorably with Culick's model. Both estimated almost the same decay constants. Using the data as input, the models showed that the decay .....

20 DISTRIBUTION/AVAILABILITY OF ABSTRACT	21 ABSTRACT SECURITY CLASSIFICATION
☒ UNCLASSIFIED/UNLIMITED ☐ SAME AS RPT ☐ DTIC USERS	Unclassified

22a NAME OF RESPONSIBLE INDIVIDUAL	22b TELEPHONE (Include Area Code)	22c OFFICE SYMBOL
Gary L. Vogt	(805) 275-5258	DYCR

DD Form 1473, JUN 86 — Previous editions are obsolete. — SECURITY CLASSIFICATION OF THIS PAGE

[illegible] associated with the absorption of sound by the injected flow were much smaller [illegible] associated with the absorption of sound by the finite admittance liner. This is not true, however, for the liner admittance values within the [illegible], which are about an order of magnitude less than the admittance of the [illegible]. Under these conditions, Culick's "flow-turning" losses become an important [illegible] the stability of solid rocket motors. The poor agreement between predicted and measured acoustic energy losses underscores the need to develop more accurate models of the acoustic energy losses associated with the injection of combustion products from the surface of solid rocket motors.

One of the important findings of this investigation is that it clearly illustrates the [illegible] using cold flow laboratory facilities to measure "flow-turning" losses. Most of the "flow-turning" absorption takes place at the finite admittance side wall of the [illegible]. Experimentally, this translates into [illegible] "flow-turning" losses as the difference between the [illegible] clever ways to get around this problem.

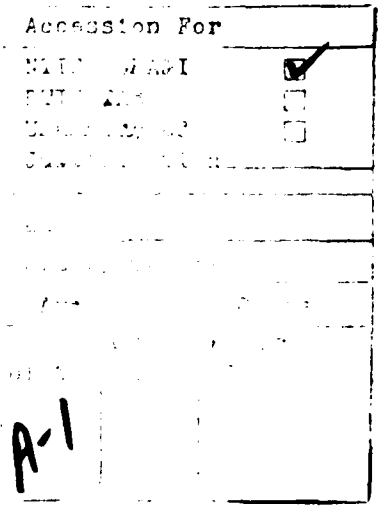

TABLE OF CONTENTS

LIST OF FIGURES

LIST OF SYMBOLS

Symbols	Definitions
A	Amplitude of sound pressure defined by Eq. (6)
A_D	Amplitude of sound pressure at downstream location
A_U	Amplitude of sound pressure at upstream location
A_w	Side-wall panel non-dimensionalized (complex) admittance
A_R	Real part of side-wall panel admittance
A_I	Imaginary part of side-wall panel admittance
c	Speed of sound
C_0	Amplitude of lower-order acoustic pressure defined by Eq. (37)
f	Frequency of sound wave
$f(x)$	Function defined by Eq. (48)
H	Distance between side-wall panels
k	Axial wave number of sound wave (ω/c)
L	Length of injection test section
M_{inj}	Mean flow injection Mach number
M_{av}	Duct cross-section averaged Mach number defined by Eq. (4)
p'	Acoustic pressure
P_{min}	Minimum amplitude of standing wave pressure defined by Eq. (9)
P_{max}	Maximum amplitude of standing wave pressure defined by Eq. (9)
R	Amplitude of reflected sound pressure;
R_D	Amplitude of reflected sound pressure downstream of injection section
R_U	Amplitude of reflected sound pressure upstream of injection section
t	time
T	Acoustic energy transmission coefficient defined by Eq. (10)
u'	Acoustic axial particle velocity
U	Axial mean flow velocity
u'	Acoustic axial particle velocity
V or v_h	Transverse injected mean flow velocity
v'	Acoustic transverse particle velocity
x	Axial distance along injection test section from upstream location
y	Transverse distance from injection test section lower side-wall panel
α	Sound energy decay constant
α_{FT}	Flow-Turning sound energy decay constant defined by Eq. (1)
ρ	Density of mean fluid
ρ'	Acoustic density
ω	Circular sound frequency ($2\pi f$)

INTRODUCTION

Solid rocket motors are considered stable if the acoustic losses within their interiors are larger than the acoustic gains. The major sources of acoustic gain and loss are, respectively, the unsteady combustion process and the convection of acoustic energy through the nozzle. In a series of pioneering analytical studies, Culick[1-4] identified the interaction between the transverse injection of mean combustion gases into the rocket interior and the longitudinal standing wave sound field as a secondary but nonetheless important source of acoustic loss. Because the interaction takes place within the motor interior where the injected flow undergoes continuous turning prior to its convection out the nozzle, these losses have been identified as acoustic "flow-turning" losses. Culick observes that during combustion, exhaust gases are injected into the rocket interior with initially zero axial acoustic momentum and exit through the nozzle with nonzero axial acoustic momentum. He argues heuristically that this increase in momentum must be acquired at the expense of an irreversible loss of acoustic energy by the mean gases within the rocket. Despite its widespread use, Culick's theoretical model appears to be misunderstood by many members of the combustion community.

The objective of this investigation is to examine Culick's model both experimentally and theoretically. The intent here is to clarify apparent misconceptions, based on a survey of the open literature, concerning its interpretations and limitations. A survey of the literature also revealed the need for further data to support Culick's claim that the injection of fluid into a chamber containing longitudinal sound results in a net absorption of sound and is hence stabilizing.

In Reference 1, Culick investigated the stability associated with the injection of fluid into a chamber containing longitudinal sound. Although the model was one-dimensional, his investigation was quite general in that it included the effects of combustion, particulate matter and variable chamber area. Since the interest here is on understanding the basis mechanics identified with "flow-turning" losses, these effects will not be investigated in this report. Instead, the far simpler problem is investigated of understanding "flow-turning" losses for the case of injection of ambient (cold) air into a channel containing longitudinal sound. Culick investigated this problem and derived the "flow-turning" expression shown below using the following assumptions:

(i) the gases are inviscid, non-heating conducting and obey the perfect gas law;
(ii) the gases were transversely injected into the chamber at very low speeds;
(iii) the chamber was closed with rigid end walls;
(iv) the chamber contained longitudinal sound.

For the interested reader, a detailed derivation of Culick's "flow-turning" losses is presented in the Appendix. Culick[4] derived the following expression for the decay constant (α_{FT}) due to the "flow-turning" losses,

$$\alpha_{FT} = -\frac{q}{2S_c E_1^2}\int_0^L \frac{m_b}{\bar{\rho}}\left(\frac{1}{k_1}\frac{dp_0}{dx}\right)^2 dx \qquad (1)$$

Equation (1) shows that the interaction between the transversely injected mean flow ($\bar{m}_b/\bar{\rho} = v_b$) – which is modelled as a source of mass at the chamber boundary in a one-dimensional formulation – and the longitudinal standing wave pattern within the chamber results in a loss of acoustic energy. Culick[2] claims that the "flow-turning" expressions (α_{FT}) "are approximate representations for the influence of essentially viscous processes in the real flow. The viscous processes occur in thin regions near the surface and are present when there is a component of unsteady motion parallel to a surface through which mass is entering or leaving." Culick apparently believes that all the "flow-turning" losses take place within this region. Although Culick never explicitly defines this "*thin region*", it is certainly reasonable to presume that it is related to the local acoustic boundary-layer thickness. In a latter paper, Culick[3] connects the "flow-turning" losses to an increase in entropy. Since the publication of his papers, Flandro[5], Vuillot and Kuentzmann[6] and Baum and Levine[7] have investigated "flow-turning" losses within the acoustic boundary-layers associated with the injection of fluid into a chamber containing sound.

Flandro, using an admittance correction acoustic "boundary-layer" type approach, extended Culick's longitudinal model to include the acoustic energy losses generated by sound waves approaching a burning wall at normal as well as grazing flow angles. He derived analytical expressions that showed that the acoustic energy losses generated from the normally directed acoustic waves were larger than the the losses generated from the grazing incident sound waves. His analysis was restricted to the edge of the viscous boundary-layer within which the mean flow direction was normal. Thus Flandro's model assumed all the acoustic energy losses occurred within this region implying that other losses associated with interactions between, say, axial mean flow gradients and the sound field within the interior away from the walls were apparently negligible. Flandro estimated the contribution of the acoustic losses from both his and Culick's model to T-Burner stability data and found that his model agreed "better" than Culick's model.

Vuillot and Kuentzmann conducted a series of experiments to examine the validity of both Culick's and Flandro's models. Test results favored the admittance correction approach adopted by Flandro. In a separate still on-going study, Baum and Levine undertook a very sophisticated computational investigation, based on solutions of the full Navier-Stokes equations of motion, of the effects of the transverse injection of air into a cylindrical tube containing longitudinal sound. They found significant sound absorption takes place within very thin regions near the tube wall where the effects of viscosity are important. These findings support Culick's hypothesis that most of the sound absorption takes place within very thin regions near the wall. They also found (i) the sound

absorption to be significantly affected by refraction induced by the gradients of the mean flow, (ii) the Richardson effect was recovered and (iii) acoustical streaming was taking place via the transfer of acoustic energy into mean flow energy. To simplify the boundary conditions, the authors assumed the tube walls, through which fluid was injected, to be acoustically rigid. Since finite admittance side walls are known to locally affect the sound field, the effect of this assumption is not known.

In support of Culick's rigid wall assumption, it is only proper to point-out that most of the researchers in this field, with the exception of Flandro, assumed that the injecting surfaces were acoustically rigid. In a real injection surface, however, the local wall admittances are finite and certainly affect the behavior of the sound fields. For example, if fluid is injected through small orifices, then the admittance of each orifice completely controls the behavior of the local sound field within a small region on the order of 2-3 orifice diameters. Unless the orifice diameters are extremely small, these regions extend beyond the local acoustic boundary-layer thickness and clearly must be accounted for in a theoretical model.

Culick[2] applied his one-dimensional "flow-turning" loss ideas to three-dimensional models. He claims that "owing to the turning of the flow near the boundary, there are contributions to the stability of waves, which do not arise in the inviscid three-dimensional analyses, but which can be estimated with the one-dimensional analysis". Culick incorporated into a three-dimensional analysis parts of his earlier derived one-dimensional "flow-turning" loss analysis. This was accomplished by adding additional one-dimensional terms to the three-dimensional formulas for the complex wave-numbers describing the two classes of problems. From his analysis of the equations describing one-dimensional complex wave-numbers, Culick derived analytic expressions for the acoustic velocity near a boundary. He modelled the general behavior of an acoustic velocity incident to a surface by partitioning it into parallel and non parallel components.

Apparently motivated by the above approach taken by Culick, Van Moorhem[8] developed a procedure to allow comparison of Culick's one dimensional wave equation to one he derived by averaging the three-dimensional wave equation over the cross-section of a motor cavity. Applying this procedure, Van Moorhem found the one-dimensional model does not contain any physical phenomena missing from the three-dimensional model and that the addition of one-dimensional "flow-turning" terms to the three-dimensional wave equation, as claimed by Culick, is inappropriate. Based on his findings, Van Moorhem claims that Culick's efforts to incorporate some of his "flow-turning" terms into a three-dimensional stability model are not warranted

It is not clear why most of the above researchers restricted their modelling and prediction of "flow-turning" losses to the acoustic boundary-layer region. Over twenty years ago, Culick[9] showed that the streamlines generated from the injection of fluid into a rocket motor penetrates into its center. If sound absorption takes place as a consequence of

the "flow-turning" process, then it appears reasonable to assume that a significant fraction of the energy loss takes place within the rocket interior and not within the acoustic boundary layer.

In an effort to substantiate Culick's model, Hersh and Walker[10] undertook an experimental program to measure "flow-turning" losses. The results of their study showed that sound was indeed absorbed by the transverse injection of air into a duct containing longitudinal sound. Test data showed that part of the sound absorption takes place at the finite admittance side walls through which the air was injected and part within the duct interior. Hersh and Walker identified refraction of the sound pressure distribution across the duct test section by the injected flow velocity gradients as a possible important contributor to the overall sound absorption. The idea here was that the refraction process increased the amplitude of the sound pressure near the wall thereby increasing the local sound absorption by the side-walls.

Hersh and Walker's investigation encountered experimental difficulties that may have compromised some of their data. In order to generate high injection flow rates into the test section, two compressors were connected in series. This caused serious compressive heating problems requiring the installation of cooling jackets to prevent the air temperatures from exceeding the safe operating limits of the B&K acoustic microphones. At the higher injection flow rates, however, the fluid temperatures were still sufficiently close to the maximum allowable values to cause concern.

Although almost the same experimental facilities used by Hersh and Walker are used in this investigation, the above experimental difficulties were avoided by using suction rather than blowing to force air into the test section. This eliminated the severe compressive heating of the air as it was injected into the test section. The experimental facilities and data acquisition and reduction scheme used in this investigation are described in Section 2. The "flow-turning" test results are presented in Section 3. The test results are compared to a one-dimensional theoretical model derived in Section 4. The important findings of this investigation are summarized in Section 5. The report closes with a detailed derivation of Culick's "flow-turning" loss expression in the Appendix.

EXPERIMENTAL PROGRAM

The objective of the experimental program was to measure the "flow-turning" losses as a function of injection flow rate and sound frequency. According to Culick's model, the sound absorption should (i) increase almost linearly with injection flow rate at low injection rates and (ii) be independent of sound frequency because the interaction takes place between the injected flow and longitudinal (plane-wave) sound. The experimental program consisted of measuring the acoustic energy flux across a test section as a function

of injection flow rate for test frequencies of 500 Hz, 1 KHz and 2 KHz. If Culick's model is valid, than sound energy should be absorbed within the injection test section. The acoustic energy flux downstream of the injection test section should be less than its corresponding upstream value. Further, the amount of energy reduction should be (1) proportional to the injection flow rate and (2) independent of the sound frequency.

The HAE two-dimensional "flow-turning" facility was used to conduct the measurements. The facility, instrumentation and data acquisition scheme are described below.

Facility Description

Figure 1 shows a scale diagram of the "flow-turning" facility. The test section consists of a 3-inch high by 2.5-inch wide rectangular cross-section duct with sidewalls constructed of high density, 1.25-inch thick Owens-Corning Glasstrate fiberglass board. This material approximates reasonably well the impedance of solid motor propellants. Air flow was supplied from two Paxton CB-95 compressors connected in series. The compressors were operated in a suction mode to avoid the compressive heating problems encountered in the earlier study by Hersh and Walker. The air flow was initially sucked into a plenum chamber located immediately below the test section. Exiting from the plenum, the airflow entered the test section via the eight outlets (four on each side) shown in Figure 1. Each side of the test section was divided into four segments, with individual air plena, control valves and flow monitoring meters allowing uniform transverse flow to be injected over the entire wetted area of the Glasstrate material. This was necessary to compare test results to a theoretical model which assumed uniform transverse injection of fluid into the test section.

Upstream of the porous-walled test section, a 3-foot long hard duct was connected to the JBL 2481 loudspeaker shown in Figure 1. The loudspeaker, used to introduce sound into the test section, was driven at frequencies of 500, 1000 and 2000 Hz by coupling an audio generator to a McIntosh 100 Watt Power Supply. Downstream of the test section, a 6-foot long duct was connected to the exponential expansion and dissipative muffler. The muffler was used to reduce the amplitude of the reflected waves as much as possible.

Both acoustic pressure and hot-wire velocity measurements were recorded. The acoustic pressures were measured using a B&K 4170 probe tube microphone for detailed surveys of the sound pressure. This instrument combines a horn coupled microphone with a self-contained preamplifier for measurements in confined spaces. This instrument was calibrated against a B&K 4134 one-half inch microphone. Entry holes for the probe microphone were drilled at appropriate locations upstream and downstream of the test section, allowing three-dimensional sampling of the standing wave patterns established within these sections.

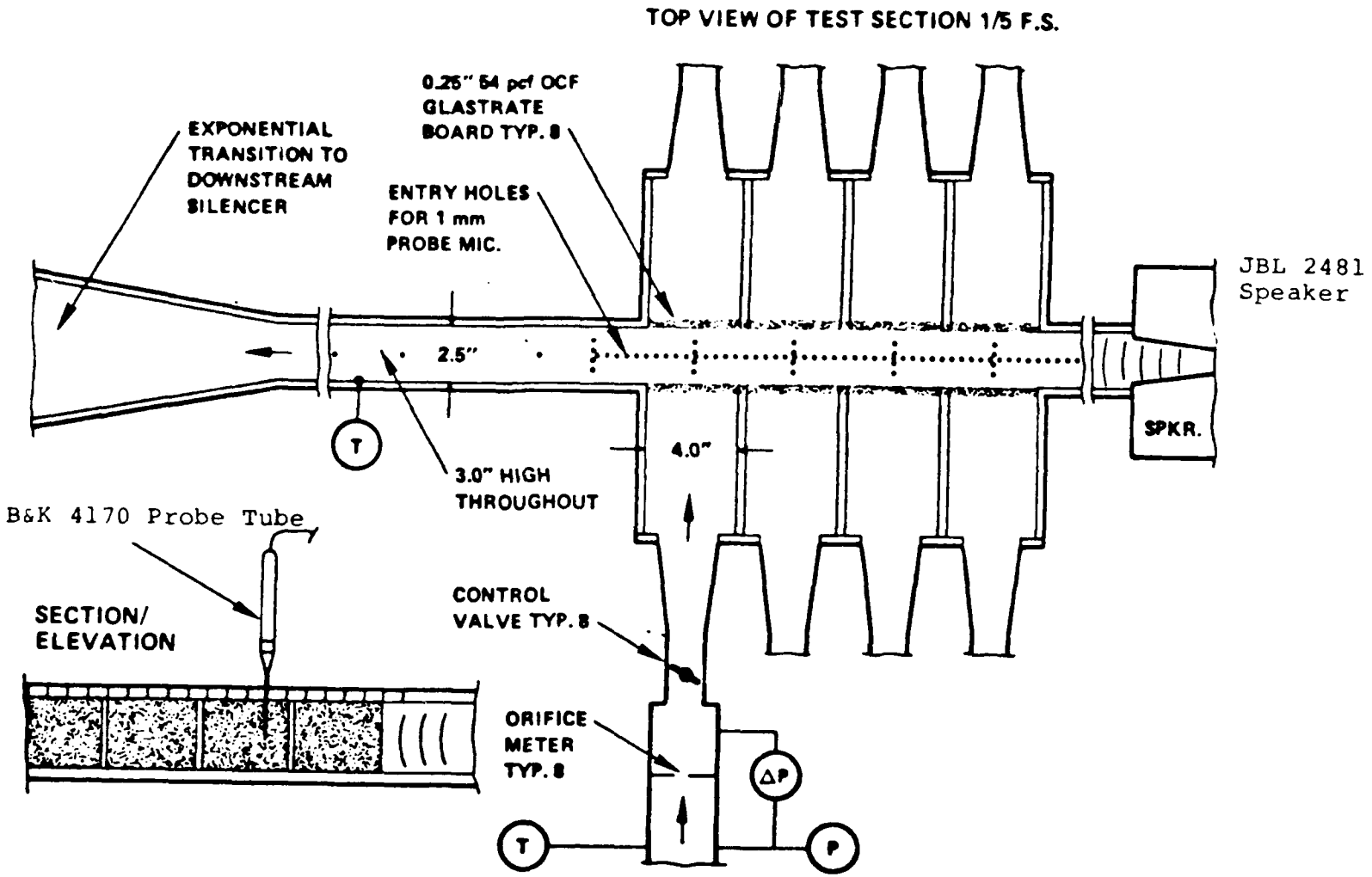

Figure 1. Schematic of HAE Flow-Turning Facility

The acoustic particle velocities were measured using a TSI 1280 hot-wire probe connected to a TSI 1054B linearized constant temperature anemometer. The hot-wire was calibrated against a pitot tube.

Data Acquisition Scheme

The data was collected and processed using a MassComp 5400 computer utilizing 16 A/D channels and 12 D/A channels having 12-bit resolution integrated into the computer to perform real time signal processing of data. MassComp developed software, Laboratory WorkBench, was used to record and analyze the data. A block diagram of the data aquisition scheme is shown in Figure 2. The A/D converter receives two signals, one of which consists of the output from a sensor [either the B&K (pressure) or TSI (velocity) instrumentation] and the other from the oscillator driving the JBL speaker (this output is not displayed in Figure 2). The signal from the sensor is phase-averaged to remove random noise generated from the turbulent flow past the sensor. A FFT of the resulting phase-averaged signal is then obtained and the resulting harmonic pressure component recorded in files for later processing and analysis.

TEST RESULTS

The test program consisted of measuring the acoustic energy flux across the injection test section as a function of injection speed and sound frequency. Only plane-wave sound was generated to simplify interpretation of the data. The test program was divided into four parts. The *first* part consisted of the measurement of the mean velocity profiles downstream of the injection test section as a function of injection flow speed. These profiles were used as input to the theoretical model presented in Section 4. The *second* part consisted of the measurement of the acoustic pressure profiles upstream and downstream of the injection test section as a function of injection speed and sound frequency. These measurements were used in the energy flux calculations. They were also used to determine the extent the sound pressure was redistributed across the test section by refraction by the injected flow velocity gradients. The *third* part consisted of the measurement of the acoustic velocity profiles downstream of the injection test section as a function of injection flow speed and sound frequency. These measurements were used as an independent check of the pressure refraction findings. The *fourth* and final part consisted of measuring the standing wave pattern upstream and downstream of the injection test section. These measurements were used to calculate acoustic energy flux. The results of these tests are presented below.

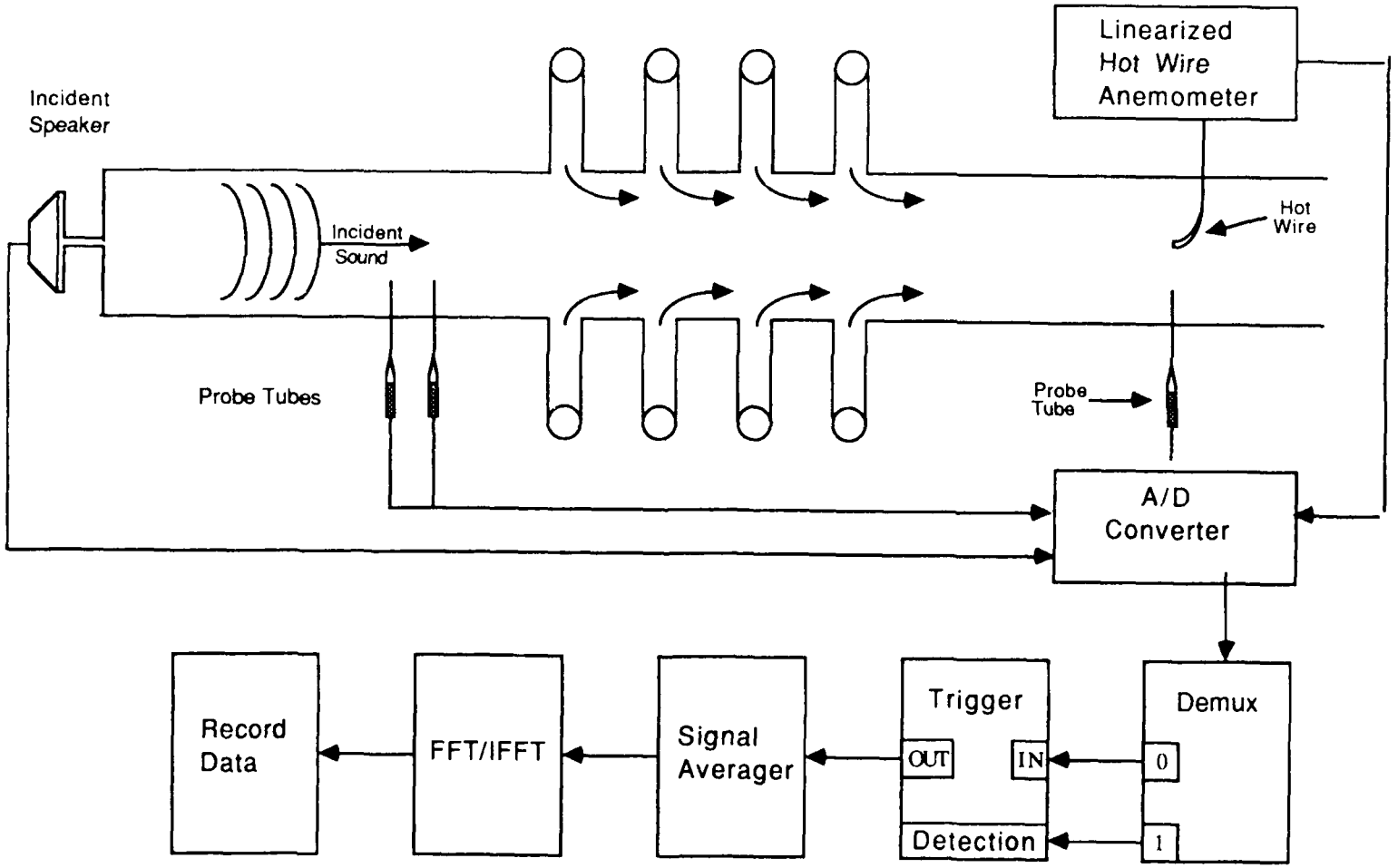

Figure 2. Block Diagram of Data Acquisition Scheme

Mean Velocity Profiles

The first task undertaken was to survey the mean velocity profiles downstream of the test section as a function of injection Mach number. A TSI-1054B linearized constant temperature anemometer was used to measure the velocity profiles. It was calibrated against a standard pitot tube before each test run to ensure its linear response against flow speed. A typical calibration curve, displayed in Figure 3, shows a linear calibration curve for flow speeds beyond about 3 m/s. Below this limit, however, the slope of the calibration curve is slightly reduced. This is probably caused by thermal conduction effects at low speeds within the facility.

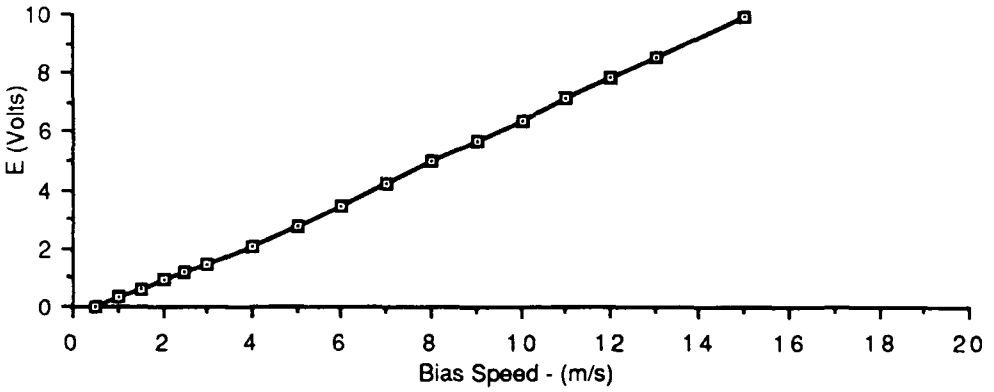

Figure 3. Calibration of Hot-Wire

The mean velocity profiles immediately downstream of the injection test section are displayed in Figure 4 as a function of injection flow speed. Observe that the flow is highly rotational with very thick regions of shear. The magnitude of the shear increases with increasing injection flow rate.

Acoustic Pressure Profiles

Measurements of the sound pressure distributions across the duct centerline – upstream and downstream of the injection test section - were undertaken to verify that only plane-wave sound was generated at the test frequencies of 500 Hz, 1 KHz and 2 KHz. The B&K Type 4170 Probe Microphone described in Section 2 was used to measure the sound pressure amplitude.

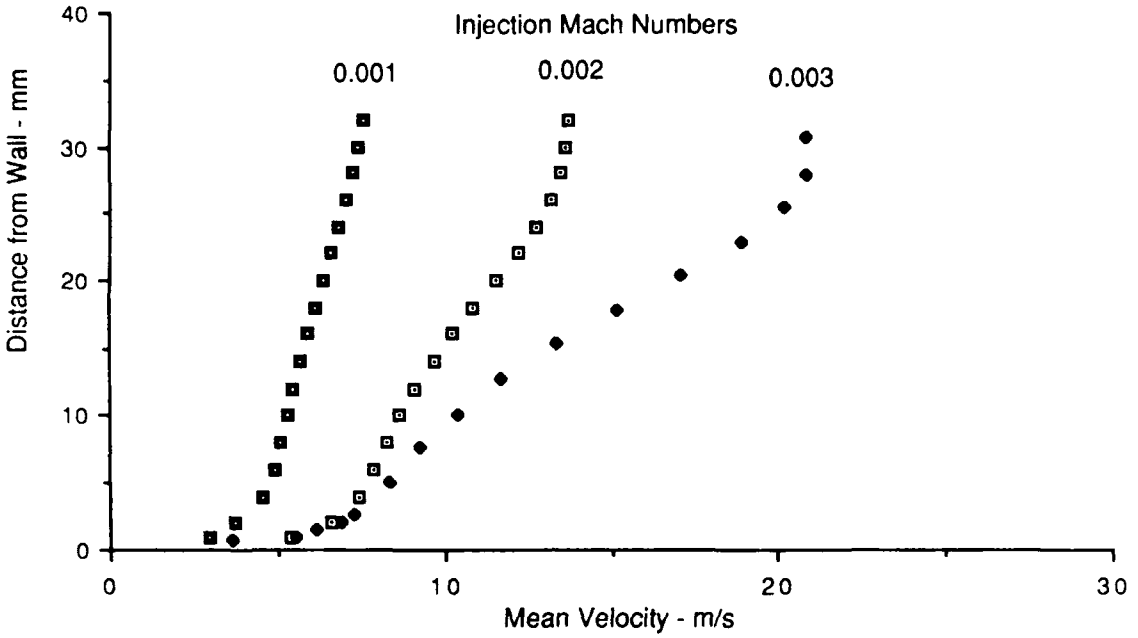

Figure 4. Downstream Mean Velocity Profiles

The results of the survey, upstream of the test section, are displayed in Figure 5. These measurements were conducted in the absence of injected flow. The acoustic pressure distributions across the duct at three different heights were recorded. The data show that plane-wave sound was generated. These results were anticipated because the frequencies were below the duct first transverse mode cut-on eigenfrequency.

The corresponding sound pressure distributions downstream of the test section were measured for injection Mach number of 0.001, 0.002 and 0.003. The interest here was whether the mean injected flow velocity gradients redistribute the sound pressure amplitudes across the test section. The redistribution of sound pressure amplitude can be explained in terms of refraction by the mean flow velocity gradients. Figure 6 illustrates the velocity refraction mechanism. For the case of downstream sound propagation, the phase speed is greater in the center than near the walls due to the mean flow profile. The higher phase speed at the center turns the wave front into the wall thereby decreasing the sound pressure at the duct center and increasing it at the wall. The converse is true for the case of upstream sound propagation. Here the sound pressure is greater in the duct center than at the wall.

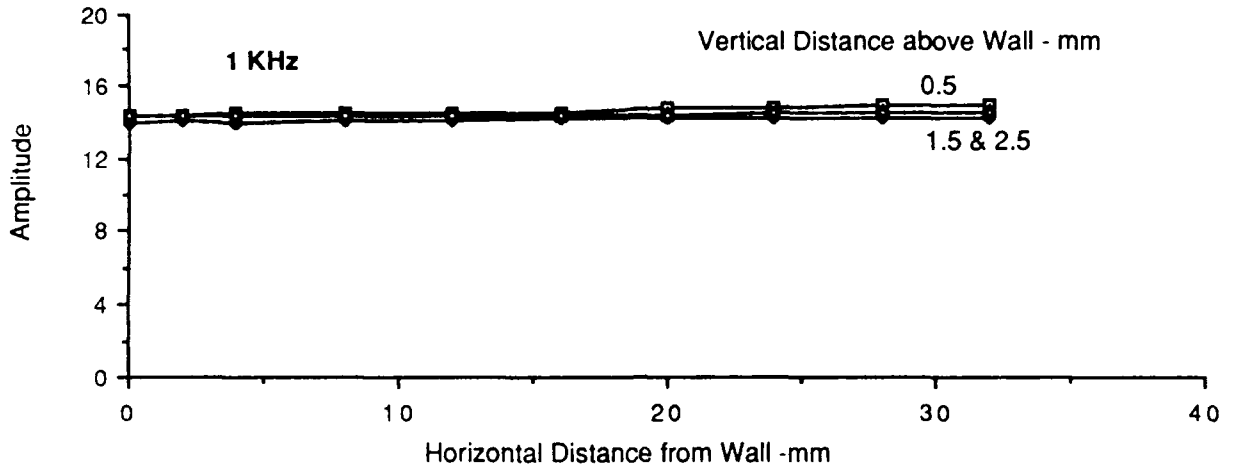

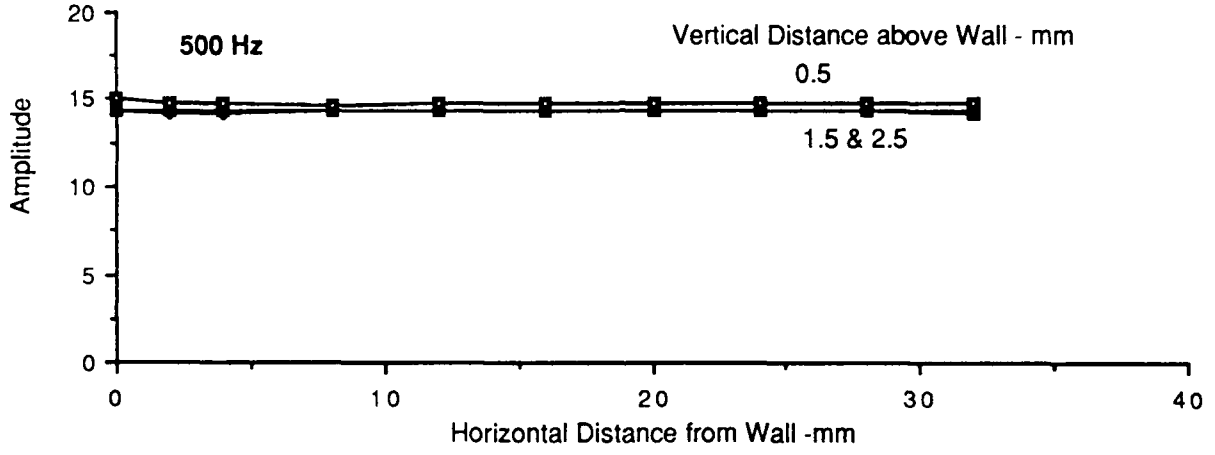

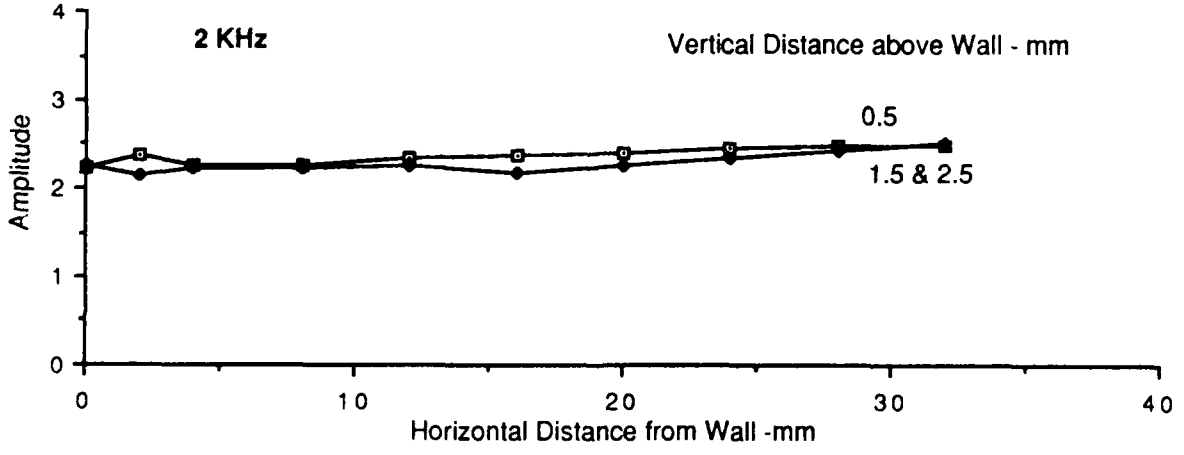

Figure 5. Upstream Acoustic Pressure Surveys - Minj = 0

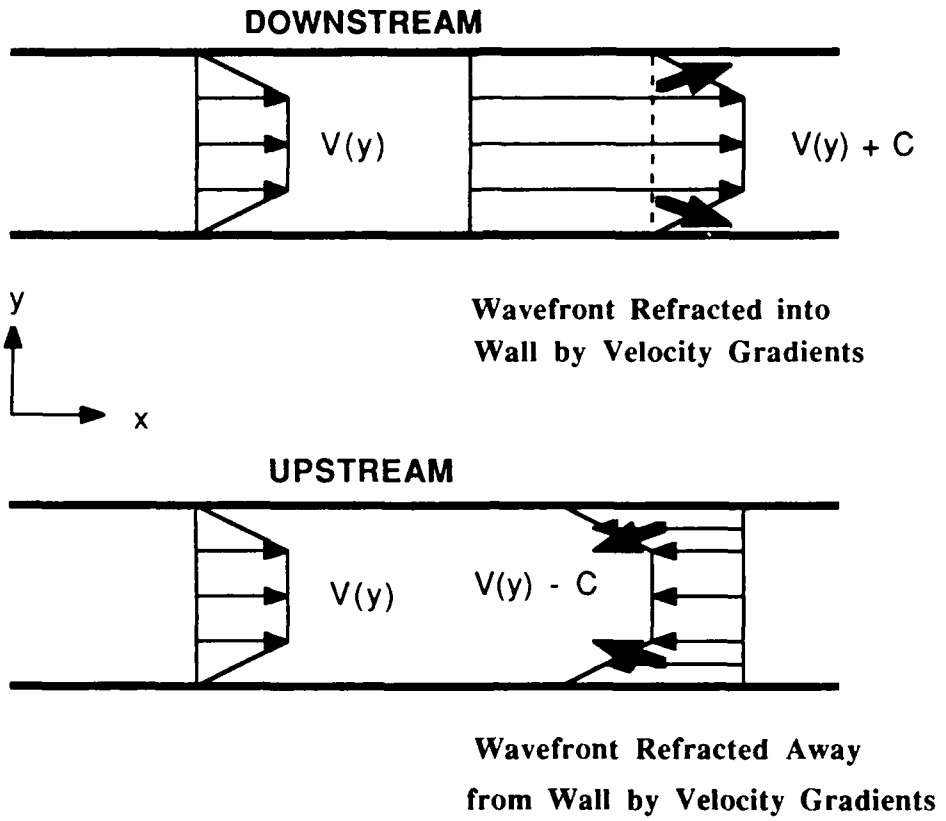

Figure 6. Schematic Showing Concept of Sound Pressure Refraction by Mean Flow Velocity Gradients

Hersh and Walker showed that the response of a probe tube microphone was strongly affected by the grazing flow past its tip. The grazing flow increases the acoustic resistance of the microphone in the same way that the resistance of a Helmholtz resonator is increased by a grazing flow. This increase in resistance results in a decrease in the response of the probe tube. The influence of the grazing flow was corrected by calibrating the B&K-4170 probe tube against a B&K-4134 one-half inch microphone. This was accomplished by flush mounting the 4134 microphone in the side wall of the HAE Wind Tunnel and positioning the 4170 probe tube in the air stream immediately in front of the 4134 as shown schematically in Figure 7. The response of the microphones was measured as a function of injection flow speed at test frequencies of 500 Hz, 1 KHz and 2 KHz. The

results of this calibration procedure are displayed in Figures 8 & 9. Figure 8 displays the ratio of flush mounted-to-probe tube sound pressure amplitude as a function of grazing flow speed for the three test frequencies. The data have been normalized by the zero speed values of each microphone and show that only modest corrections are necessary, the largest being about 9% for the 1 KHz data. Figure 9 shows the corresponding phase corrections representing the differences in phase between the 4134 and 4170 microphones. As shown, these corrections are also modest.

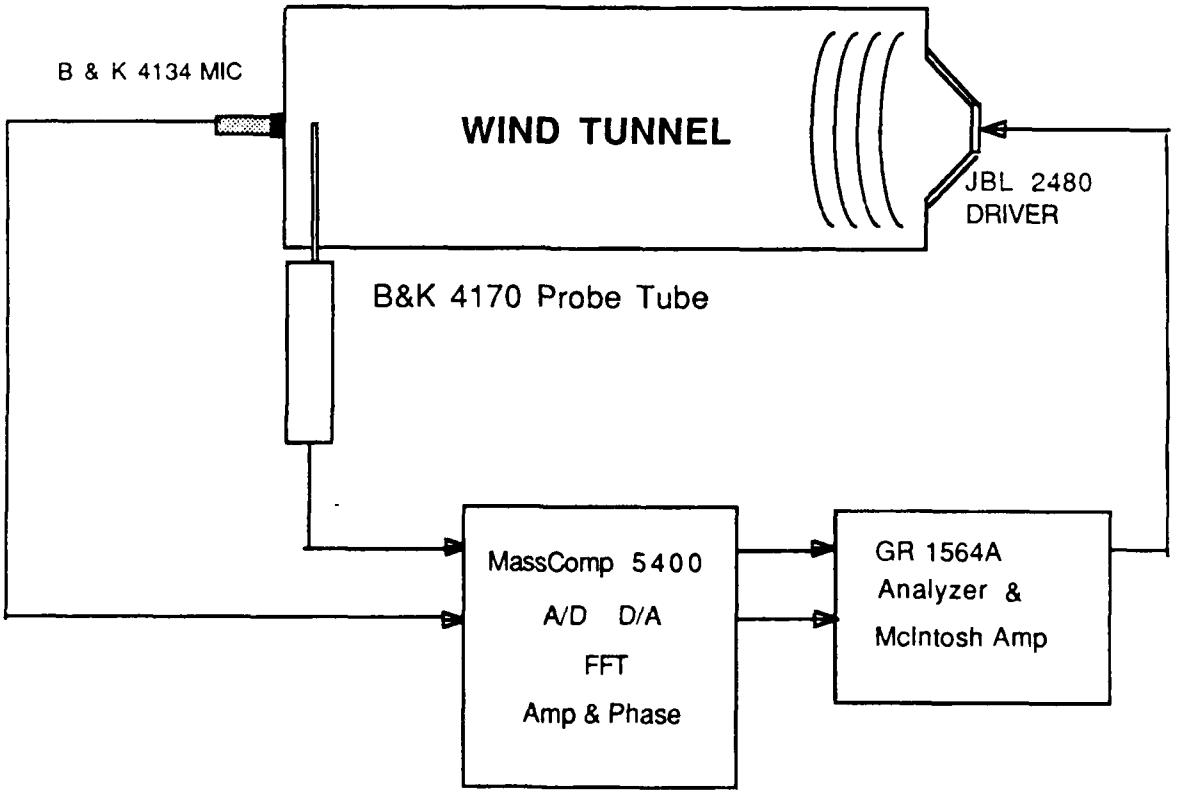

Figure 7. Schematic Of Calibration Of B&K 4170 Probe Tube

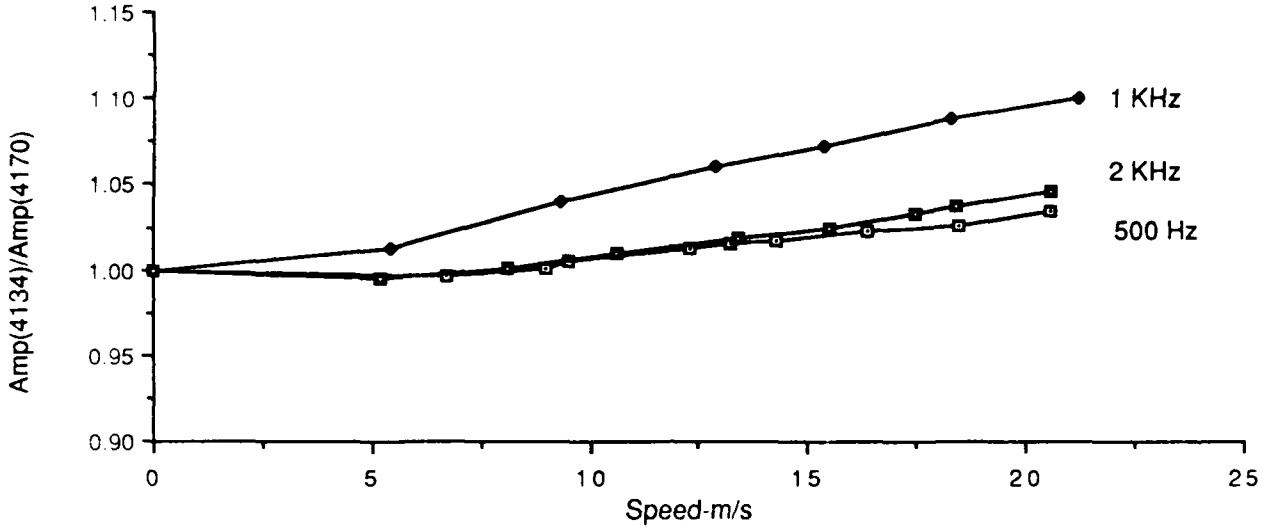

Figure 8. Calibration of Amplitude Response of Probe Tube

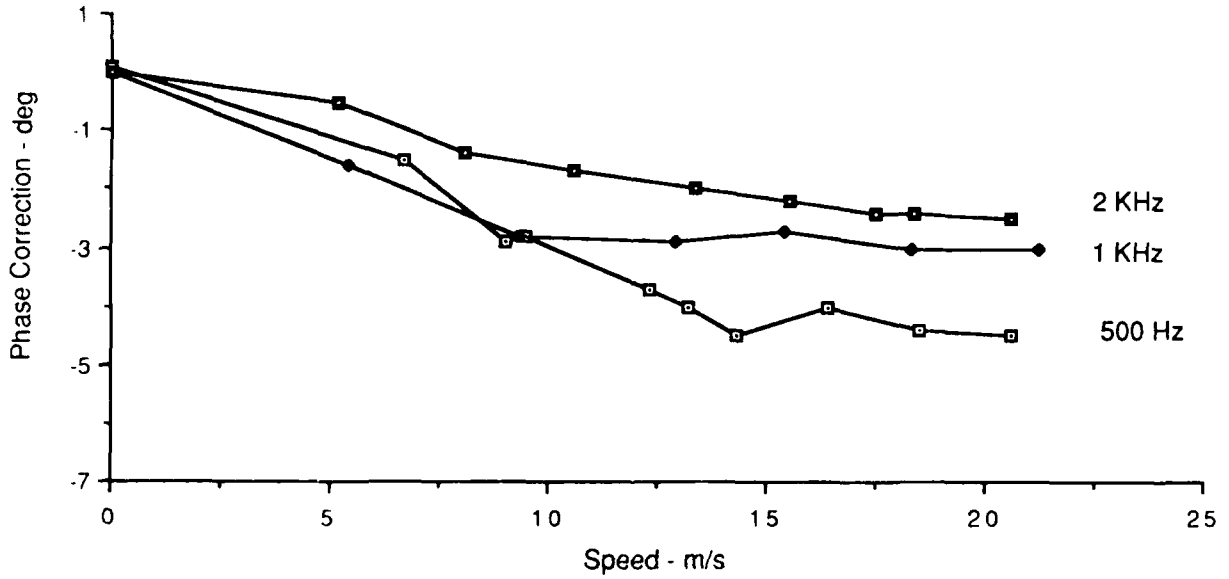

Figure 9. Calibration of Phase Response of Probe Tube

Preliminary measurements showed the 4170 probe tube to be sensitive to mean flow speed and mean flow shear. To avoid extensive calibration of the probe tube, the B&K UA-0385 bullet shaped nose cone was attached to a B&K-4136 one-quarter inch microphone to measure the sound pressure profiles downstream of the test section. As displayed in Figures 10 & 11, only plane-wave sound was generated across the test section, even for the maximum injection Mach number tested of 0.003. Thus the effects of refraction by the mean flow velocity gradients were negligible - at least for the range of injection flow speeds tested.

The acoustic pressure measurements presented above suggest that plane-wave motion exists throughout the test section. Additional sound pressure surveys were conducted in the vertical direction (see Figure 1) to verify that the sound field is planar over the entire duct cross-section. The B&K 4170 probe tube was used to measure the amplitude and phase distributions in the vertical direction within the injection test section exit plane. The results of the pressure survey, presented in Figures 12 & 13 for the three test frequencies, show that the acoustic motion throughout the entire injection test section is planar.

Acoustic Velocity Profiles

The TSI hot-wire anemometry system was used to measure the acoustic particle velocity profile across the test section to provide an independent verification that the sound wave refraction by the mean flow velocity gradients was indeed negligible. The idea here is that for sound fields governed by linear acoustics, a linear relationship exists between the sound pressure p' and the particle velocity u', i.e. $p' \sim u'$. Thus, both the acoustic pressure and velocity profiles should be planar. Preliminary measurements were conducted to verify that $p' \sim u'$. The amplitudes of p' and u' were measured as a function of speaker input voltage, the results of which are plotted in Figure 14 for frequencies of 500 Hz, 1 KHz and 2 KHz. Observe that both p' and u' increase *linearly* with sound pressure amplitude which is proportional to speaker input voltage.

The linear response of both these measurements verified that the hot-wire measured acoustic velocities. The acoustic particle velocity profiles across the test section, displayed in Figures 15 & 16, show that the sound is plane-wave in support of the findings displayed in Figures 10 & 11. The data near the wall is not accurate because the hot-wire output is not accurate when the mean flow velocity is small.

Acoustic Energy Transmission Measurements

According to Culick's "flow-turning" model, the interaction between transversely injected mean flow and longitudinally excited plane-wave sound results in a net absorption of sound. To substantiate his findings, an acoustic energy exchange concept (AEE) is

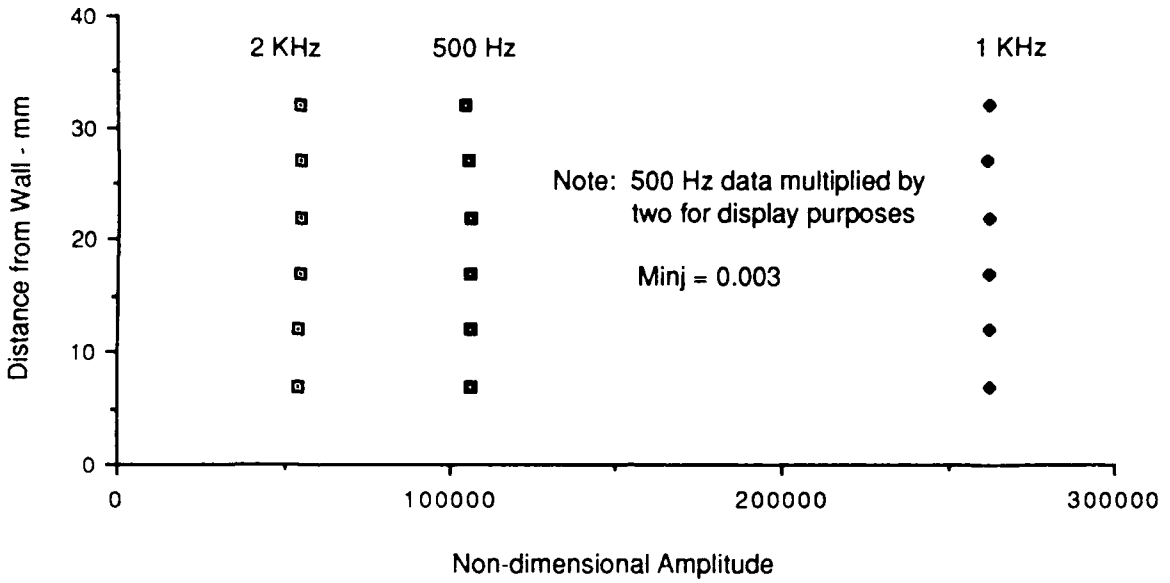

Figure 10. Downstream Sound Pressure Amplitude Survey

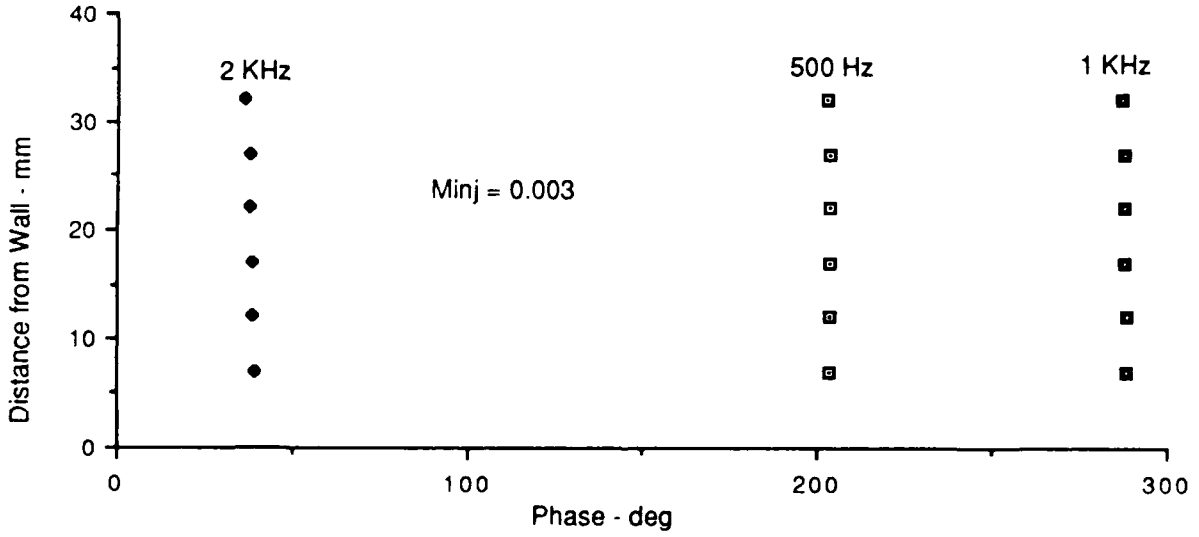

Figure 11. Downstream Sound Pressure Phase Survey

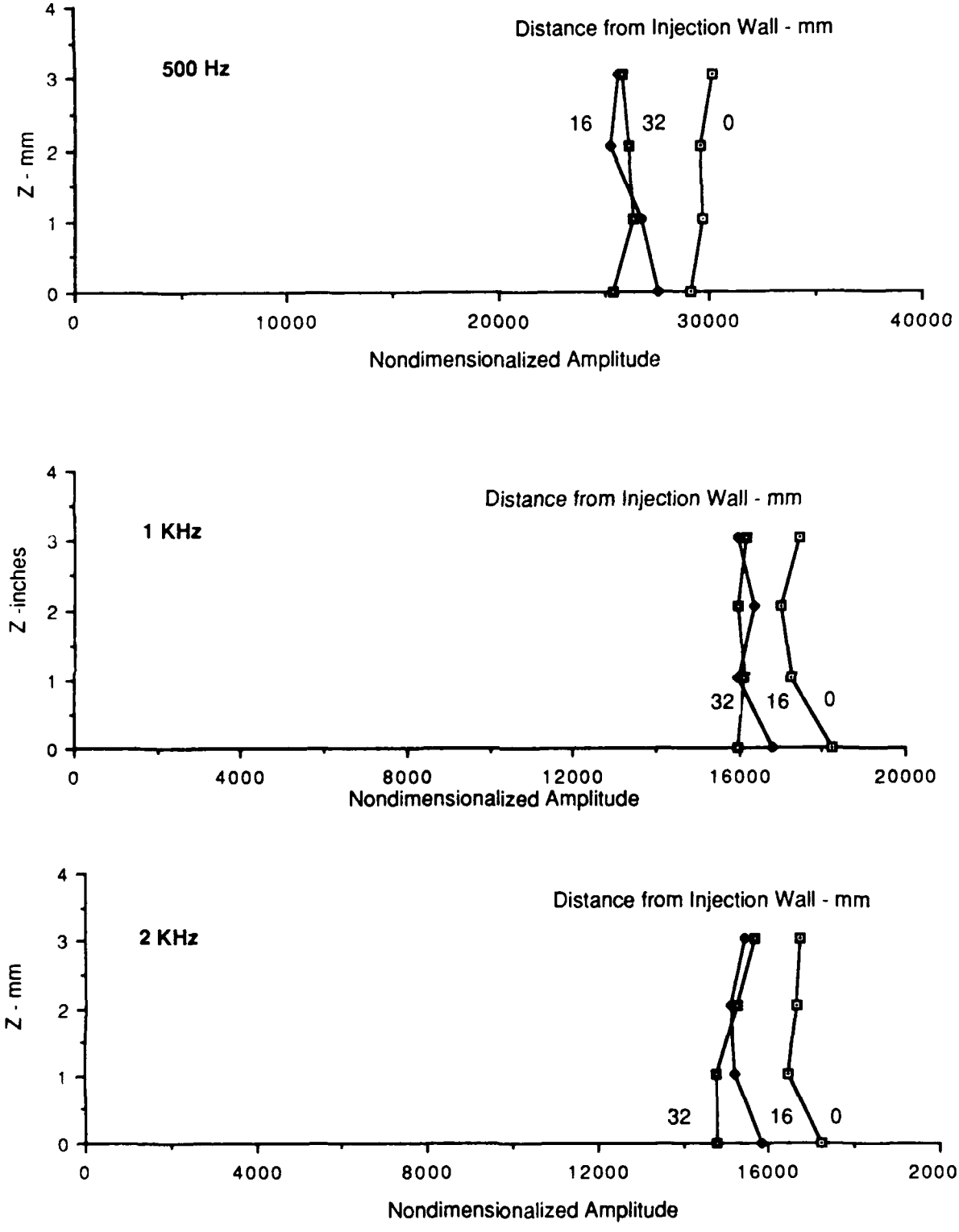

Figure 12. Vertical Sound Amplitude Profile - Minj = 0.003

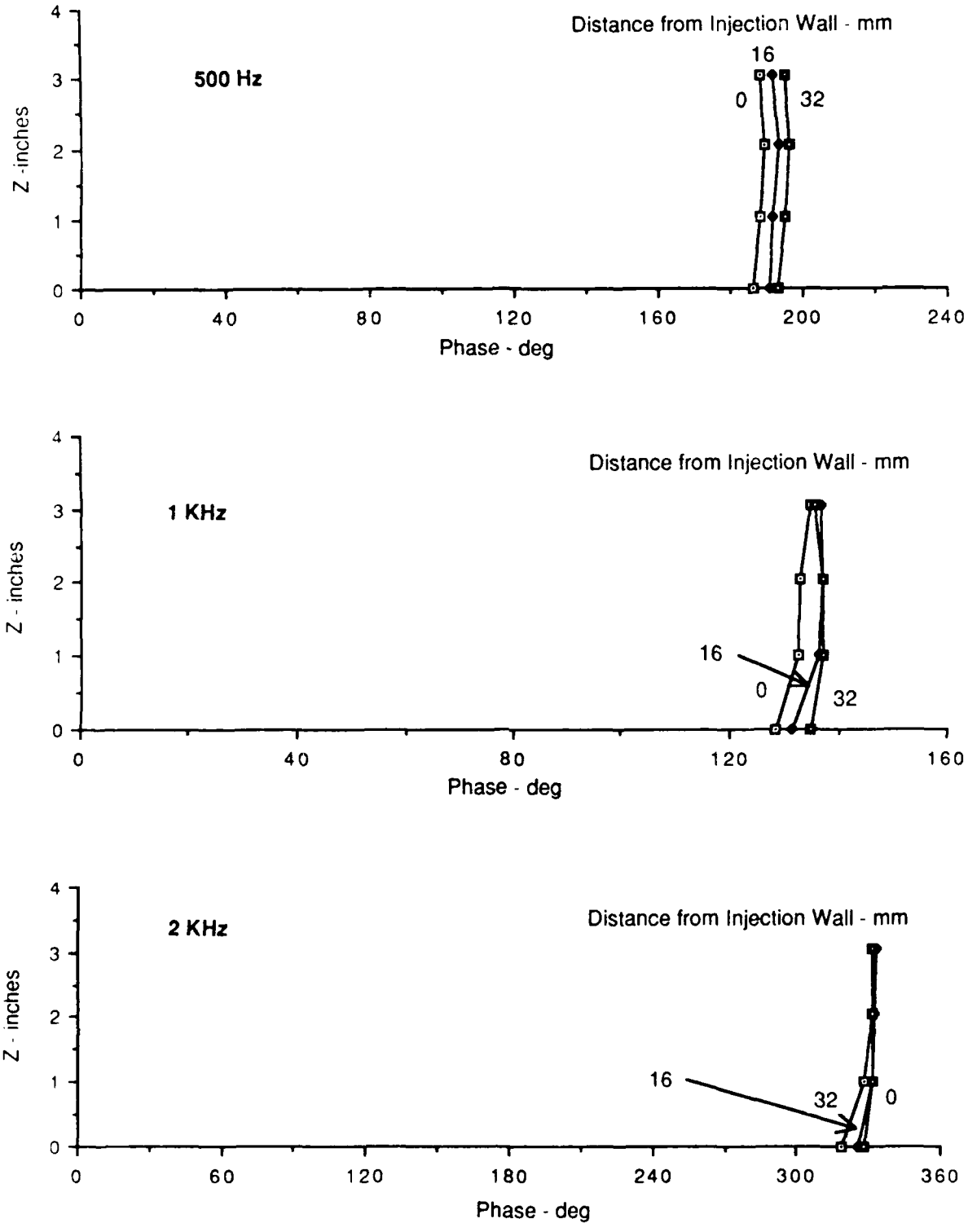

Figure 13. Vertical Sound Phase Profile - Minj = 0.003

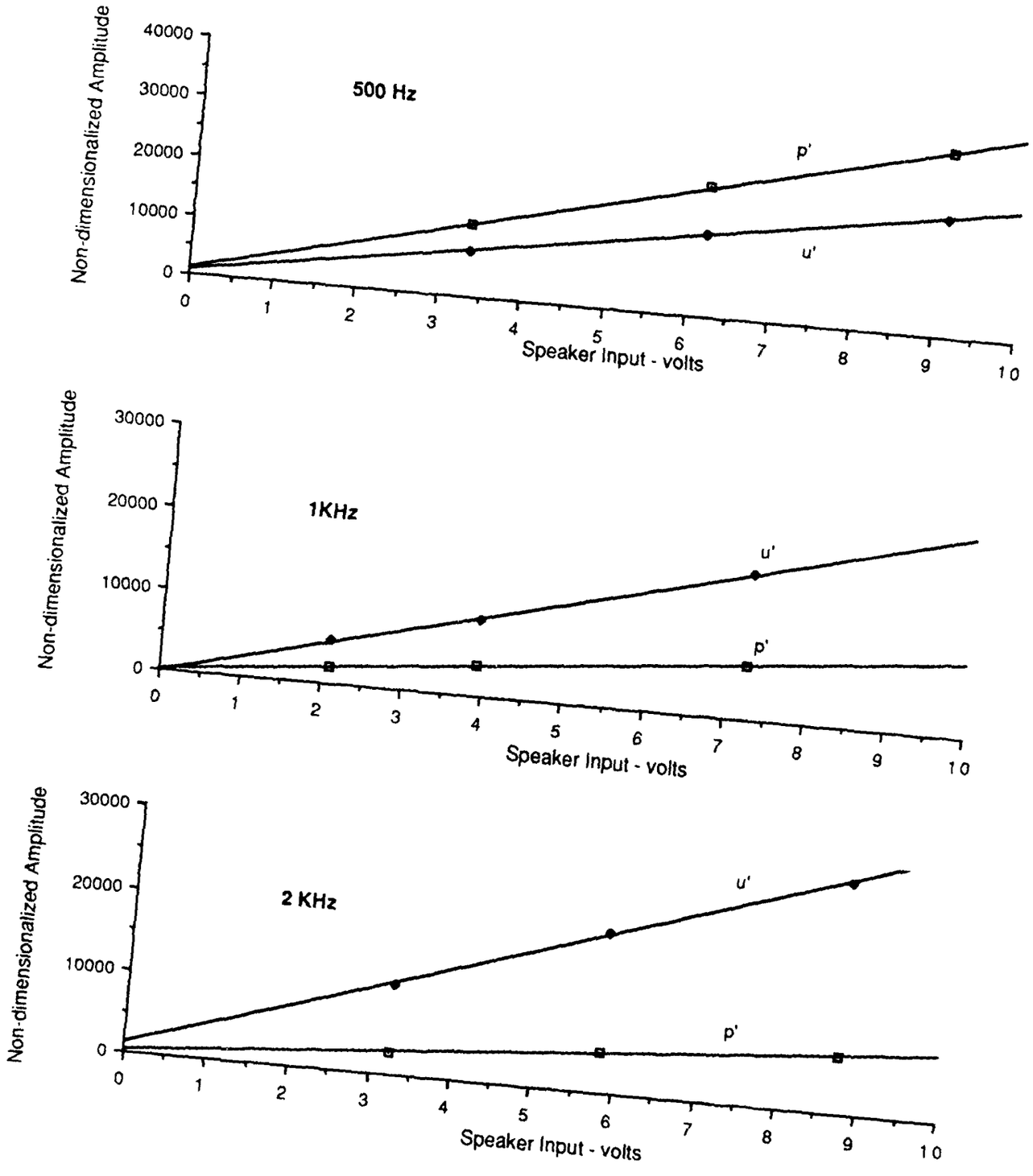

Figure 14. Calibration of Acoustic Response of Hot-Wire

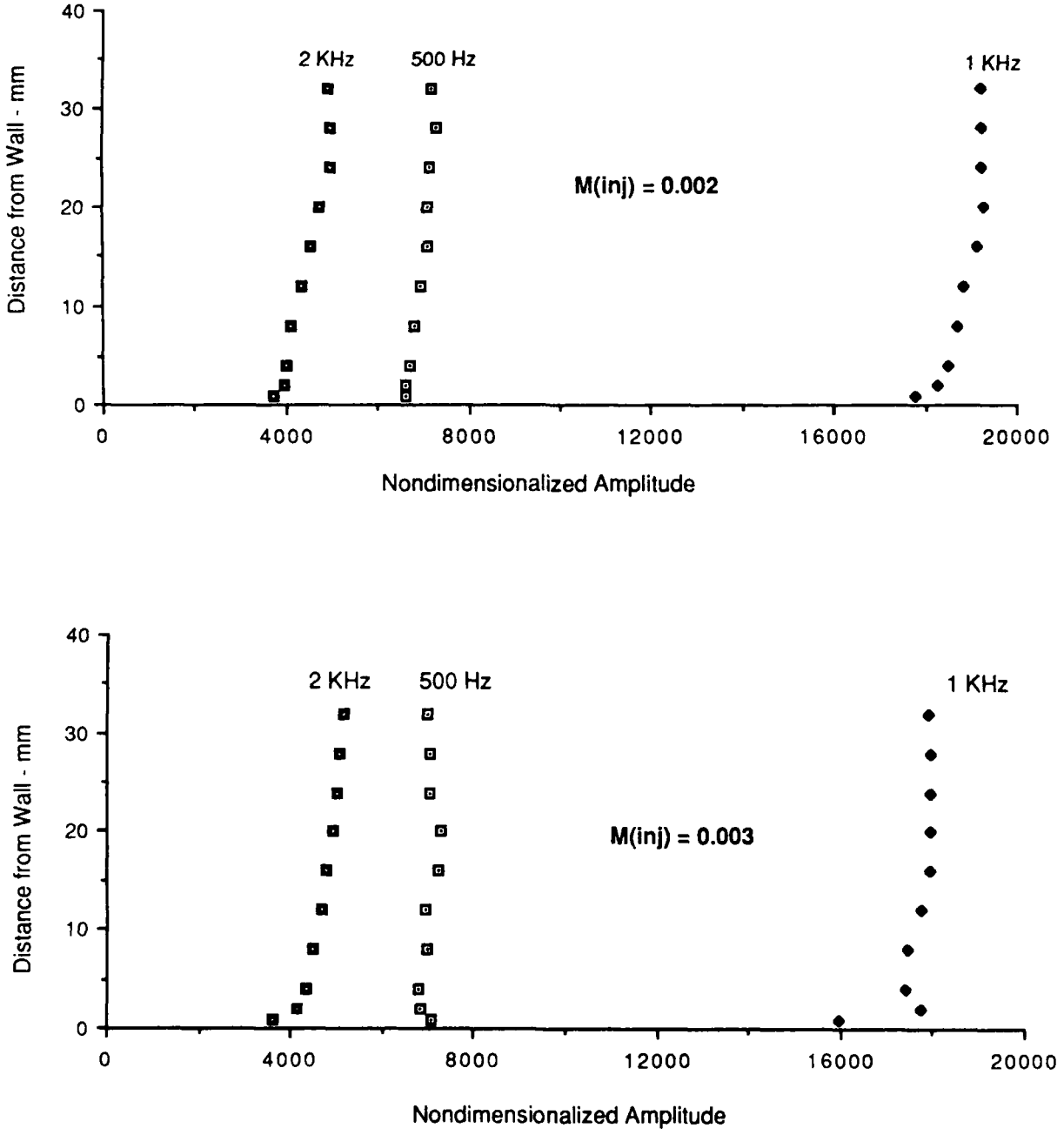

Figure 15. Downstream Acoustic Velocity Amplitude Profiles

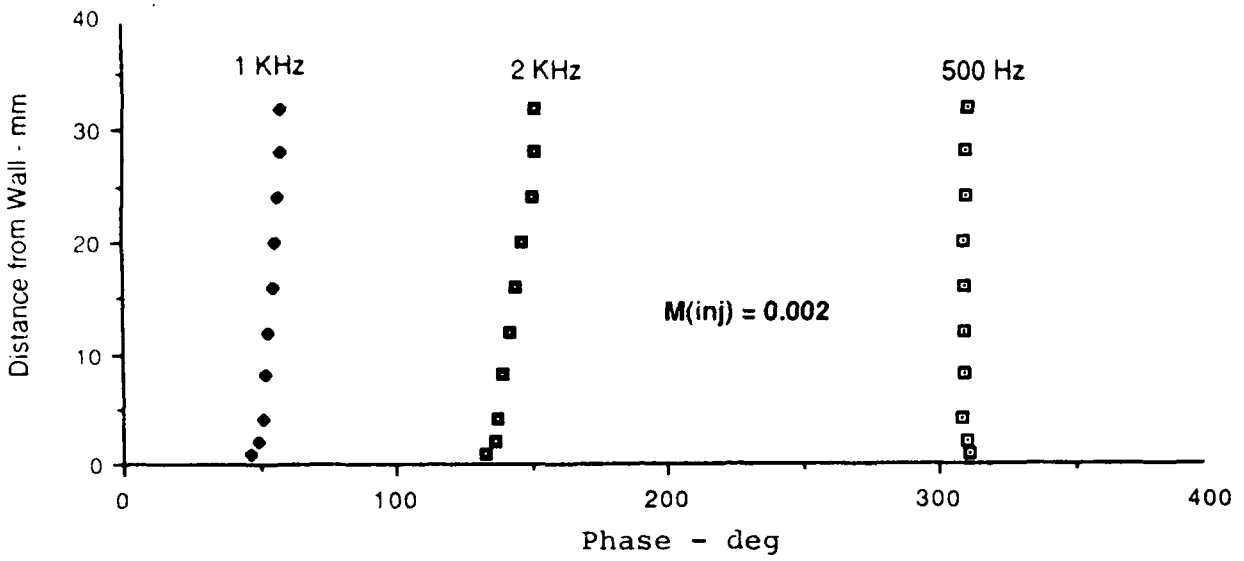

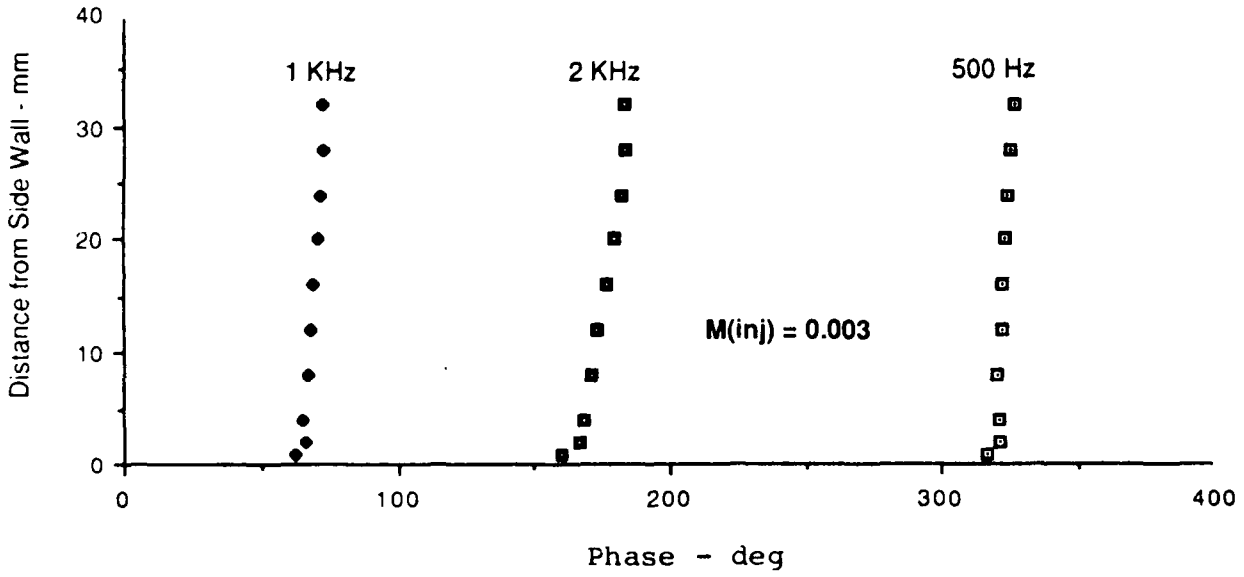

Figure 16. Downstream Acoustic Velocity Phase Profiles

introduced below defined as the difference between the acoustic energy transmission coefficient (T) across the test section with and without injected mean flow,

$$AEE \equiv T(M_{inj}) - T(0) \tag{2}$$

Here $T(M_{inj})$ is the acoustic energy transmission coefficient across the test section defined as

$$T(M_{inj}) \equiv 10Log\left[\frac{p_R(L, M_{inj})u_R(L, M_{inj})}{p_R(0, M_{inj})u_R(0, M_{inj})}(1 + M_{av})\right] \tag{3}$$

where p_R and u_R represent the real parts of the root-mean-square (rms) acoustic pressure and velocity respectively and M_{av} is the average Mach number across the duct defined as

$$M_{av} \equiv \frac{1}{H}\int_0^H M(y)\,dy \tag{4}$$

The parameter H is the duct width and M(y) is the mean flow Mach number distribution across the duct cross-section displayed in Figure 3. The term $1+M_{av}$ in Eq.(3) accounts for the additional energy convection of the sound field by the mean flow[11].

Since the data presented in Section 2.3 showed that the sound field across the injection test section was planar, the acoustic pressures and velocities are evaluated at the duct center (y=32 mm). This simplifies enormously the time and effort required to conduct the acoustic energy transmission loss measurements. The rms quantities in Eq. (3) are defined in the usual way as

$$p_R(x, M_{inj}) \equiv \sqrt{\frac{1}{T}\int_0^T [p_R(x, t, M_{inj})]^2 dt} \tag{5}$$

The B&K 4170 probe tube was used to measure the sound pressure standing wave patterns upstream and downstream of the injection test section for sound frequencies of 500 Hz, 1 KHz and 2 KHz and for injection Mach numbers of 0.001, 0.002 and 0.003. Test results, uncorrected for the effects of grazing flow past the probe tube, are displayed in Figures 17-22. As shown, curve-fits of the data are superimposed. The curve-fits were

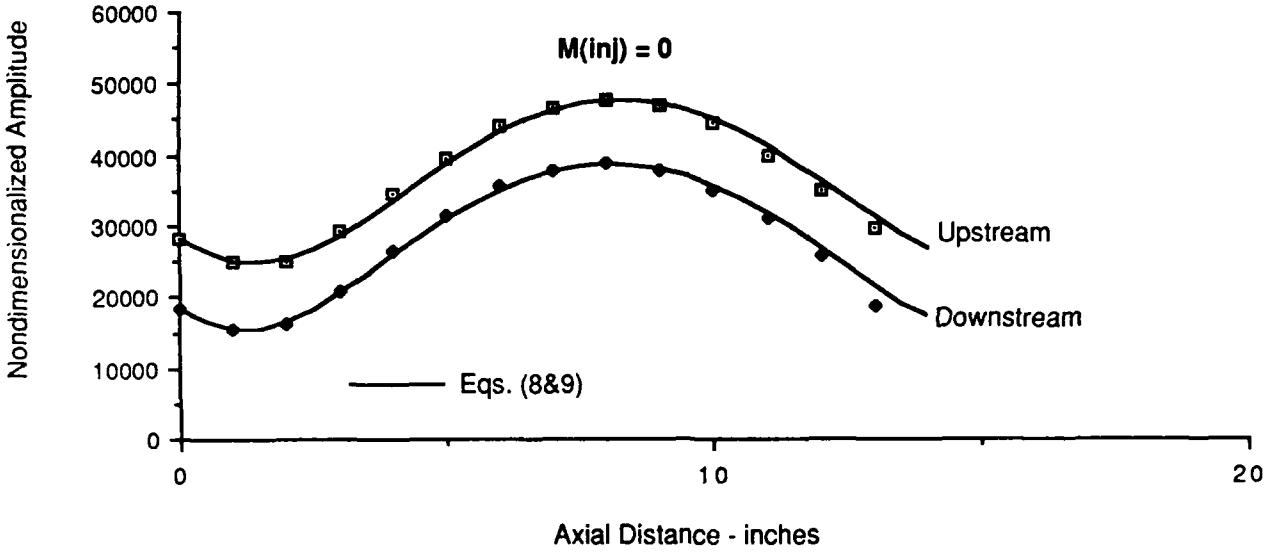

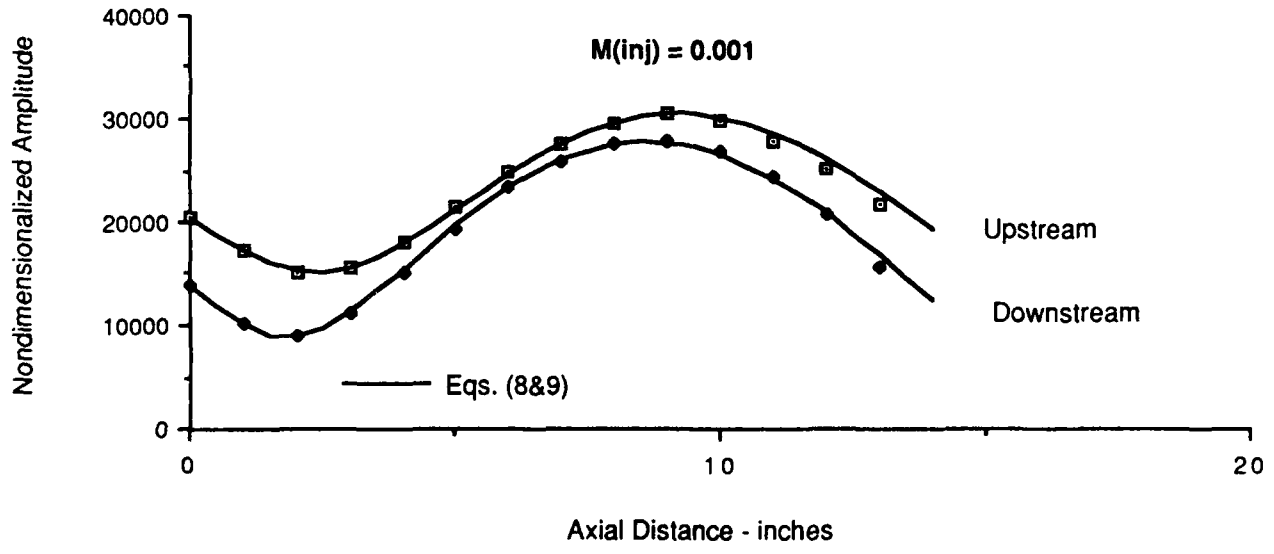

Figure 17. Curve-fit of Standing Wave Pattern for 500 Hz

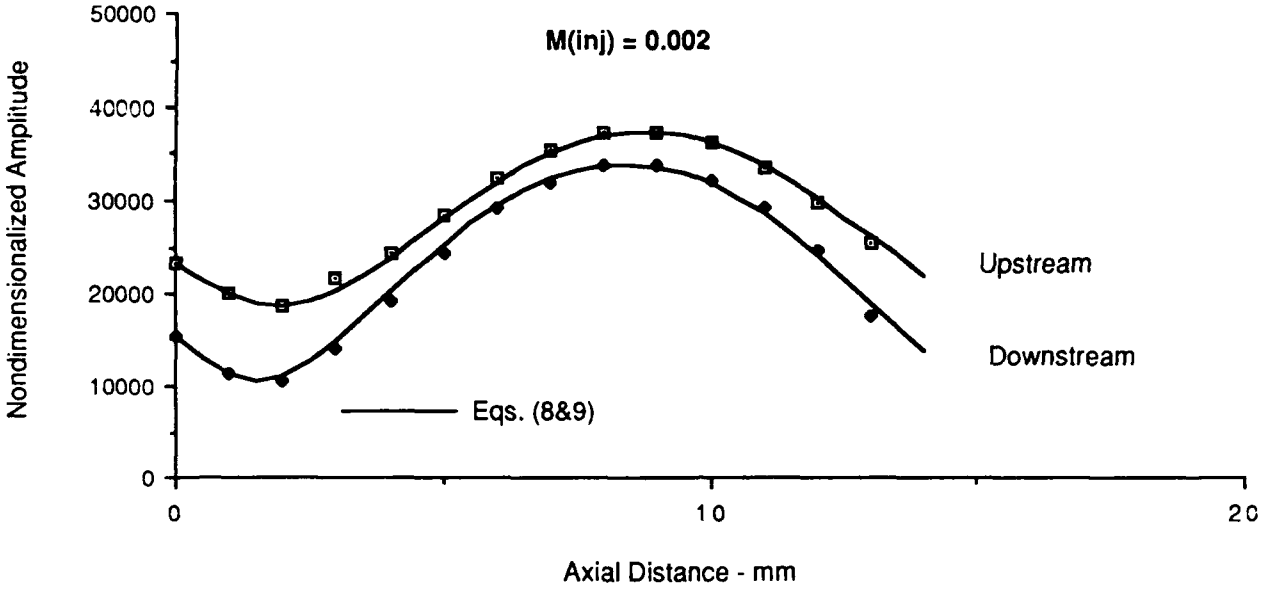

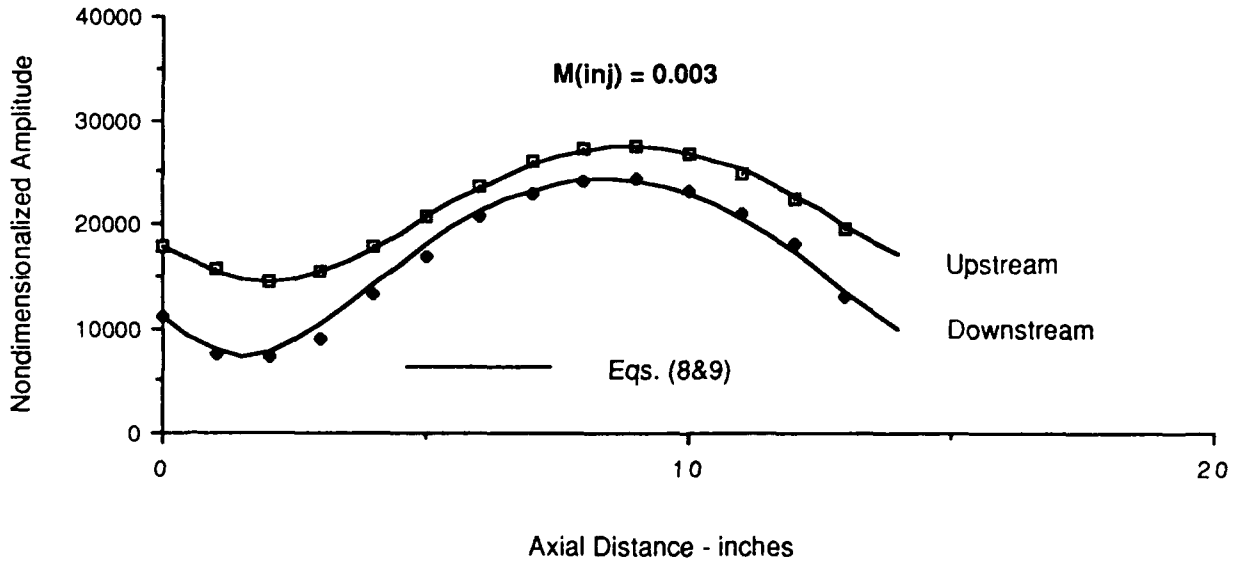

Figure 18. Curve-fit of Standing Wave Pattern for 500 Hz

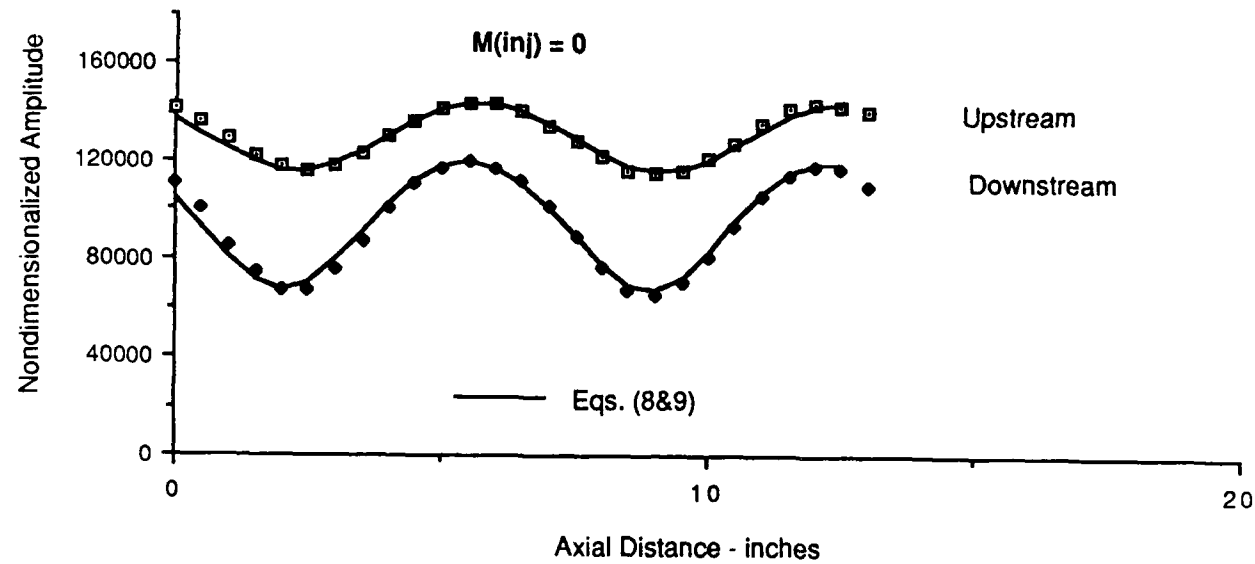

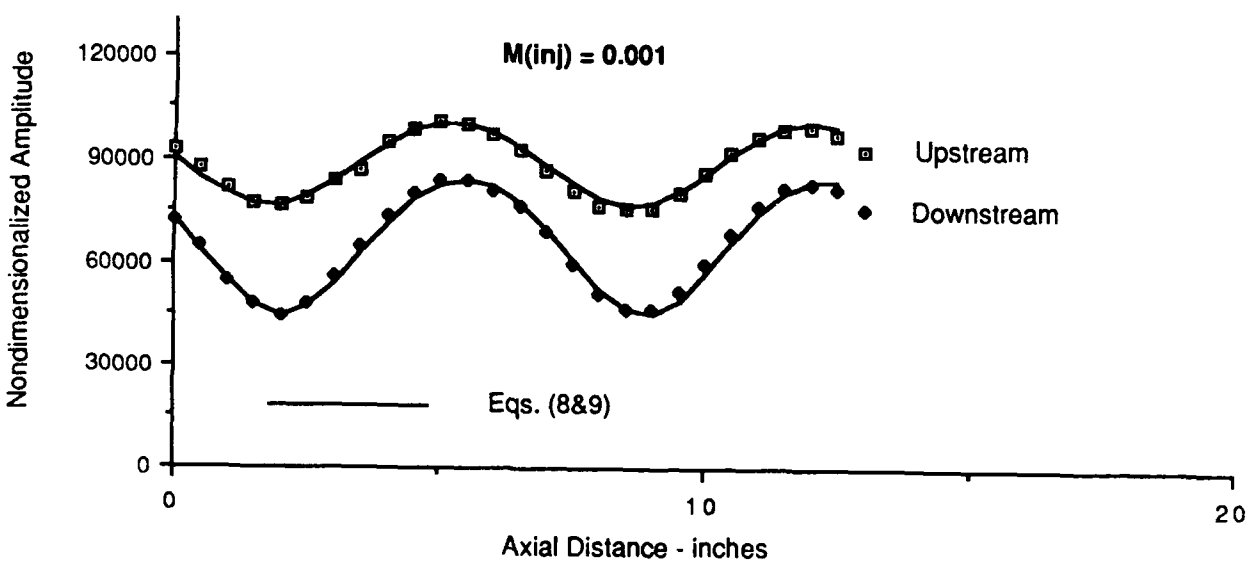

Figure 19. Curve-fit of Standing Wave Pattern for 1 KHz

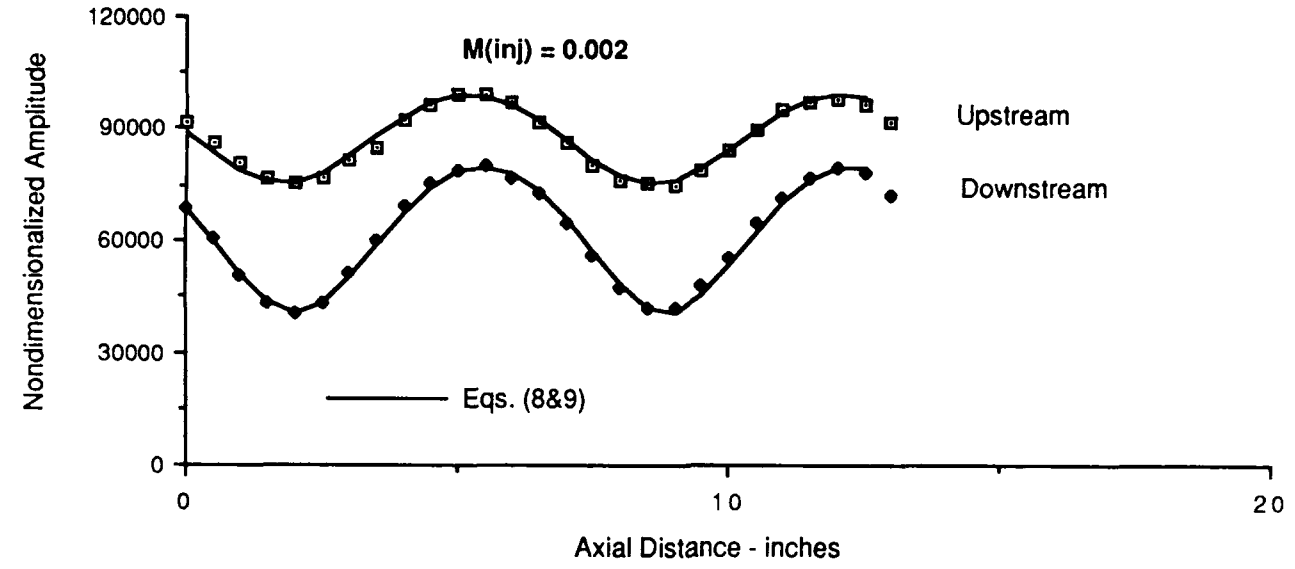

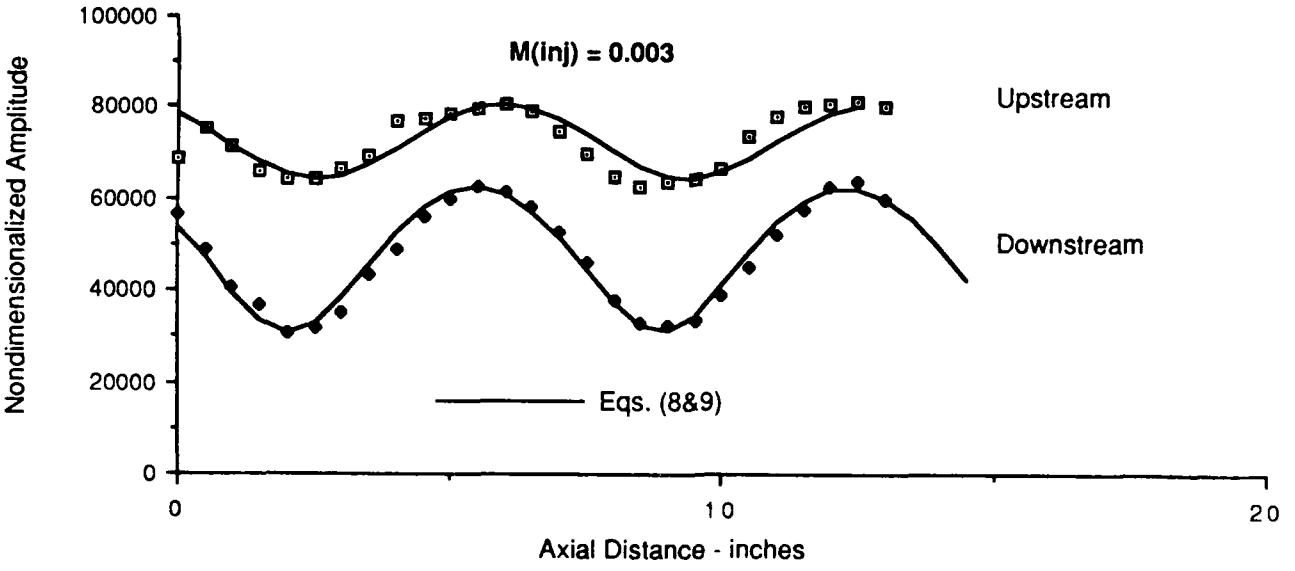

Figure 20. Curve-fit of Standing Wave Pattern for 1 KHz

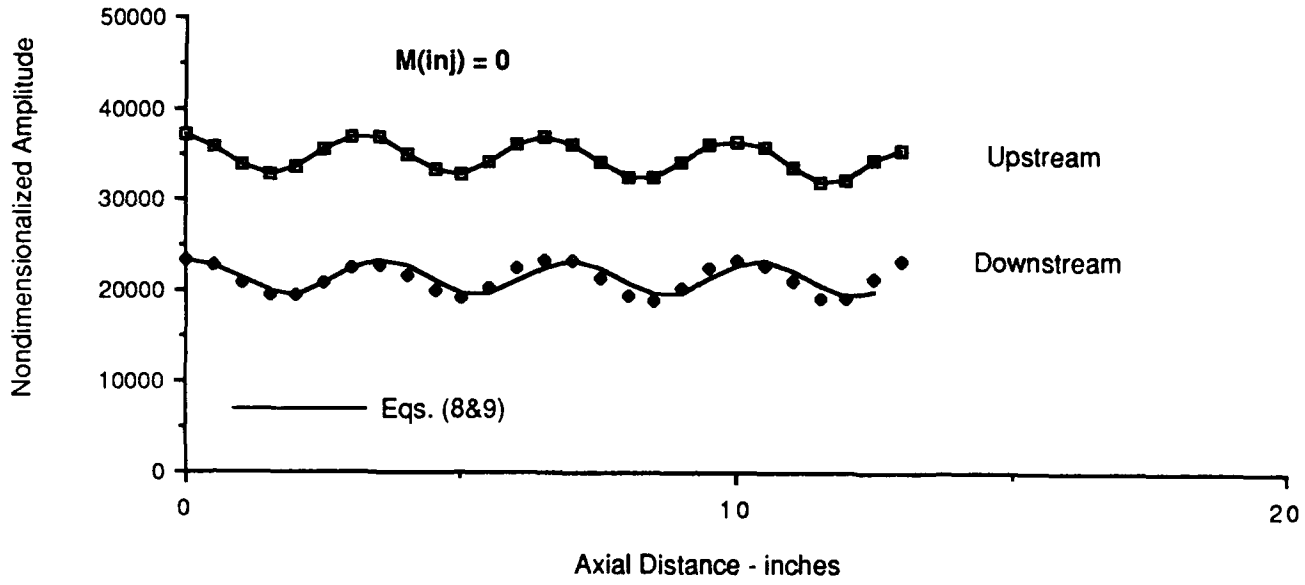

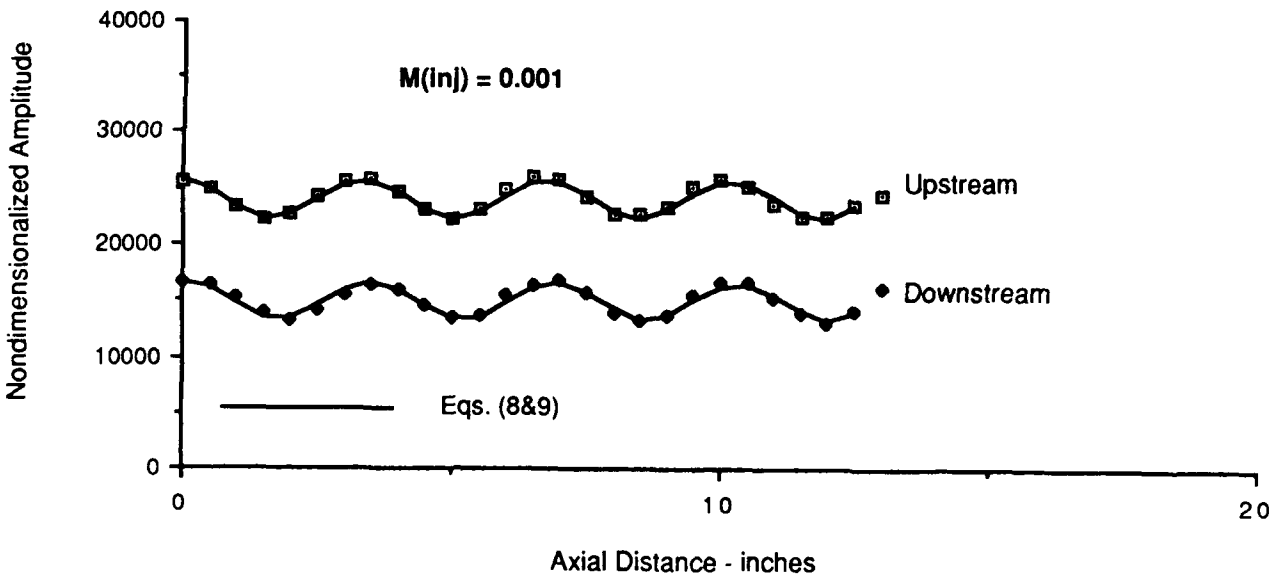

Figure 21. Curve-fit of Standing Wave Pattern for 2 KHz

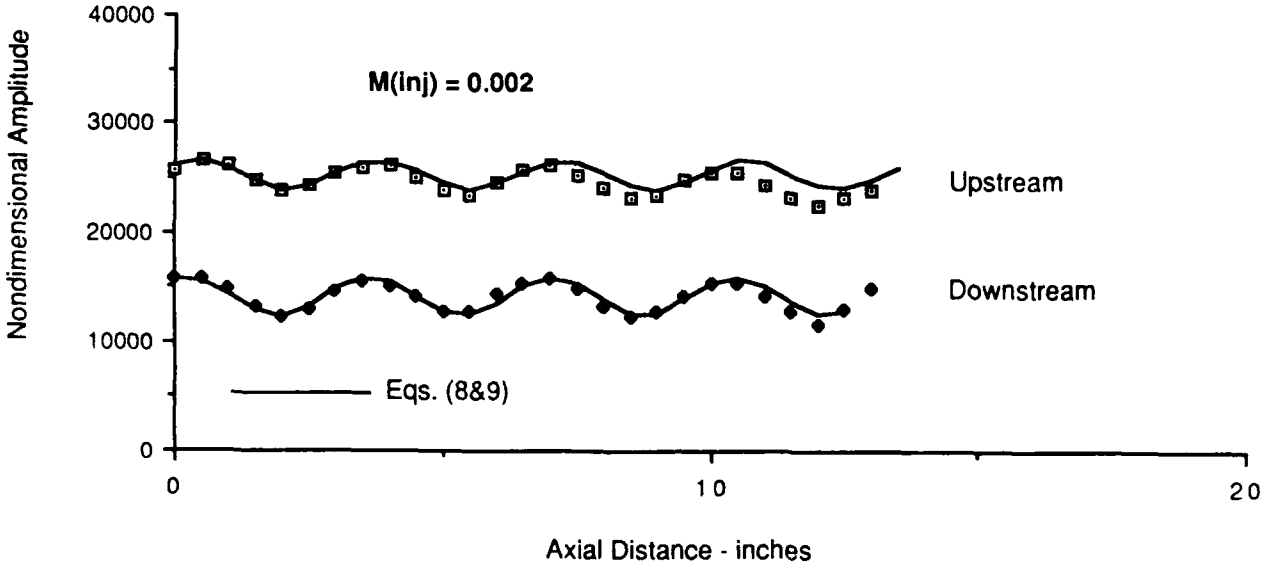

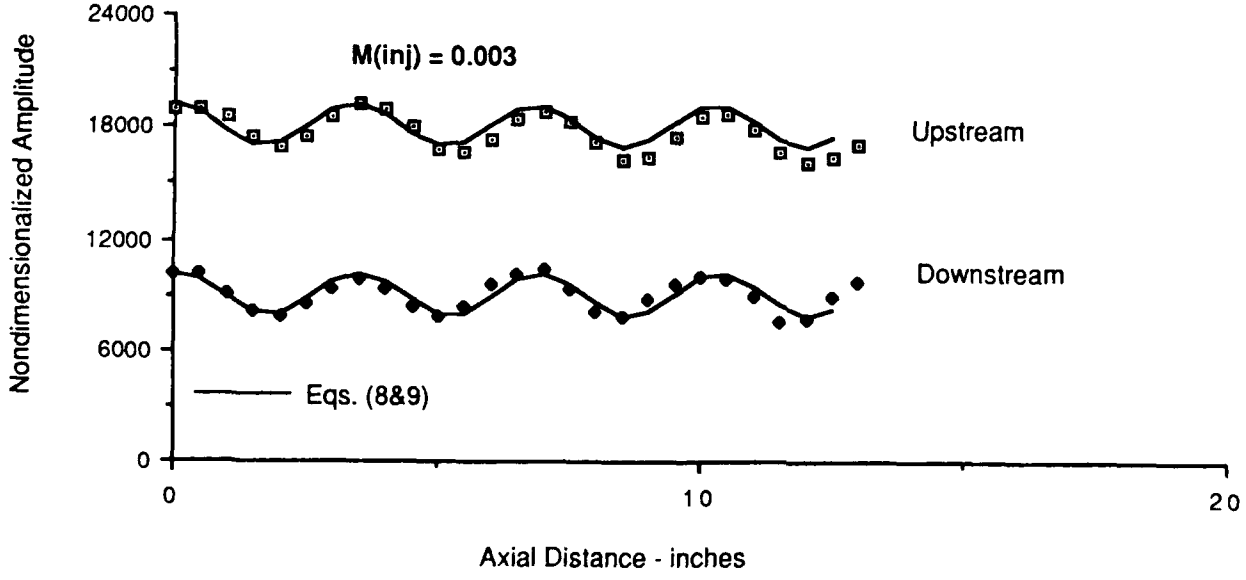

Figure 22. Curve-fit of Standing Wave Pattern for 2 KHz

derived starting from the following standard one-dimensional solution of the sound pressure containing incident and reflected components in a moving fluid,

$$p(x,t) = A\left[e^{i\left(\omega t - \frac{kx}{1-M_{av}}\right)} + Re^{i\left(\omega t + \frac{kx}{1+M_{av}} + \phi\right)}\right] \tag{6}$$

where A is the amplitude of the incident sound pressure, R is the ratio of the amplitudes of the incident and reflected waves, ϕ is the phase of the reflected wave and $k = \omega/c$. The corresponding one-dimensional sound particle velocity is

$$u(x,t) = \frac{A}{\rho c}\left[e^{i\left(\omega t - \frac{kx}{1-M_{av}}\right)} - Re^{i\left(\omega t + \frac{kx}{1+M_{av}} + \phi\right)}\right] \tag{7}$$

The following rms sound pressure (p_{rms}) is derived from Eqs. (5 & 6),

$$p_{rms}(x) = A\sqrt{1 + R^2 + 2R\cos\left(\frac{2kx}{1-M_{av}^2} + \varphi\right)} \tag{8}$$

Observe from Eq. (8) that minimums (P_{min}) occur whenever $2kx+\phi = \pi + 2\pi n$, and maximums (P_{max}) occur whenever $2kx+\phi = 2\pi n$ where n is an integer. Using this, it is straight-forward to show that

$$A = \frac{P_{min} + P_{max}}{2}; \qquad R = \frac{P_{max} - P_{min}}{P_{max} + P_{min}}; \qquad \phi = \pi - \frac{2kx_{min}}{1-M_{av}^2} \tag{9}$$

The final estimate of the standing wave pressures upstream and downstream of the injection test section (see Fig. 1) follows upon substituting Eq. (9) into Eq. (8). As shown in Figures 17-22, the agreement between predicted and measured standing wave patterns is excellent. Incorporating the above definitions into Eq. (3) yields the following expression for the acoustic energy transmission T across the injection test section,

$$T(M_{inj}) = 10 \log\left[\frac{A_D^2(L, M_{inj})\left(1 - R_D^2\right)(1 + M_{av})}{A_U^2(0, M_{inj})\left(1 - R_U^2\right)}\right] \qquad (10)$$

The acoustic energy transmission depends only upon the amplitude A of the incident wave, the coefficient R of the reflected wave and the mean flow average Mach number. Here, A_D & A_U represent the amplitudes of the sound pressures downstream (x=L) and upstream (x=0) of the injection test section respectively. Table 1 summarizes the parameters A and R for the twenty-four test cases. The downstream amplitudes A_D are corrected for the effects of the grazing flow past the tip of the B&K 4170 Probe Tube. These corrections were provided by the amplitude calibration curves shown in Figure 8. Substituting these corrections along with the other parameters displayed in Table 1 into Eq. (10) results in the acoustic energy transmission values summarized in Figure 23 and Table 2.

The results show, for the three frequencies tested, a slight acoustic energy gain for injection Mach numbers between 0 < Minj < 0.1. Beyond Minj = 0.1, the data shows virtually little change for frequencies of 500 Hz and 1 KHz but over 1 dB of loss at 2 KHz. This is more clearly defined in Figure 24 which was derived using the acoustic energy exchange definition of Eq. (2). What may be happening here is that at very low injection Mach numbers, the absorption of sound energy may be too little to off-set the increase in energy due to mean flow convection $1+M_{av}$ as indicated in Eq. (10). This may explain the slight acoustic energy gain. At the higher injection flow Mach numbers, however, the "flow-turning" losses may increase more rapidly than the convection term resulting in the small losses shown in Figures 23 & 24. If this explanation is valid, it suggests that the "flow-turning" losses are not controlled by terms proportional to the first power of M_{inj}, as Culick's linear analysis predicts, but instead exhibits a quadratic or higher power dependence upon M_{inj}. Regardless of the details of the sound absorption process, it seems reasonable to conclude from the measurements presented in Figures 23 & 24 that the "flow-turning" process indeed absorbs sound. This absorption is certainly very small relative to the absorption by the finite admittance side walls (at $M_{inj} = 0$).

THEORETICAL MODEL

The development of a detailed one-dimensional theoretical model was undertaken to extend Culick's rigid wall derivation to include the effects of finite admittance (i.e., absorbing) walls. The interest here is to identify and rank order the various interactions among the injected flows, longitudinal sound fields and finite admittance walls. Another equally important objective is to examine the value and utility of the one-dimensional model by comparing its predicted absorption to the measured data presented in Section 3.

Table 1. Summary of Uncorrected Standing Wave Pattern Test Results

Frequency (Hz)	Minj	Upstream A	Upstream R	Downstream A_{unc}	Downstream R
500	0	36,344	0.315	27,100	0.429
	0.001	22,830	0.335	18,350	0.513
	0.002	27,800	0.334	22,211	0.525
	0.003	20,975	0.310	15,830	0.539
1 KHz	0	129,300	0.115	92,404	0.296
	0.001	88,622	0.134	64,520	0.305
	0.002	87,124	0.137	60,120	0.329
	0.003	72,493	0.113	46,750	0.338
2 KHz	0	34,551	0.075	21,170	0.106
	0.001	24,010	0.073	14,840	0.106
	0.002	24,992	0.061	13,889	0.113
	0.003	17,917	0.072	9,031	0.129

Table 2. Summary of Transmission Measurements

Frequency (Hz)	M_{inj}	Downstream A_{uncorr}	Downstream A_{corr}	$T(M_{inj})$ (dB)	Acoustic Energy Exchange - (dB)
500	0	36,344	27.100	-2.98	0.00
	0.001	22,830	18,405	-2.62	0.36
	0.002	27,800	22,544	-2.60	0.38
	0.003	20,975	16,432	-3.02	-0.04
1 KHz	0	129,300	92,404	-3.26	0.00
	0.001	88,622	66,843	-2.73	0.53
	0.002	87,124	64,449	-2.92	0.54
	0.003	72,493	52,313	-3.16	0.10
2 KHz	0	34,551	21,170	-4.28	0.00
	0.001	24,010	14,899	-4.11	0.17
	0.002	24,992	14,167	-4.86	-0.58

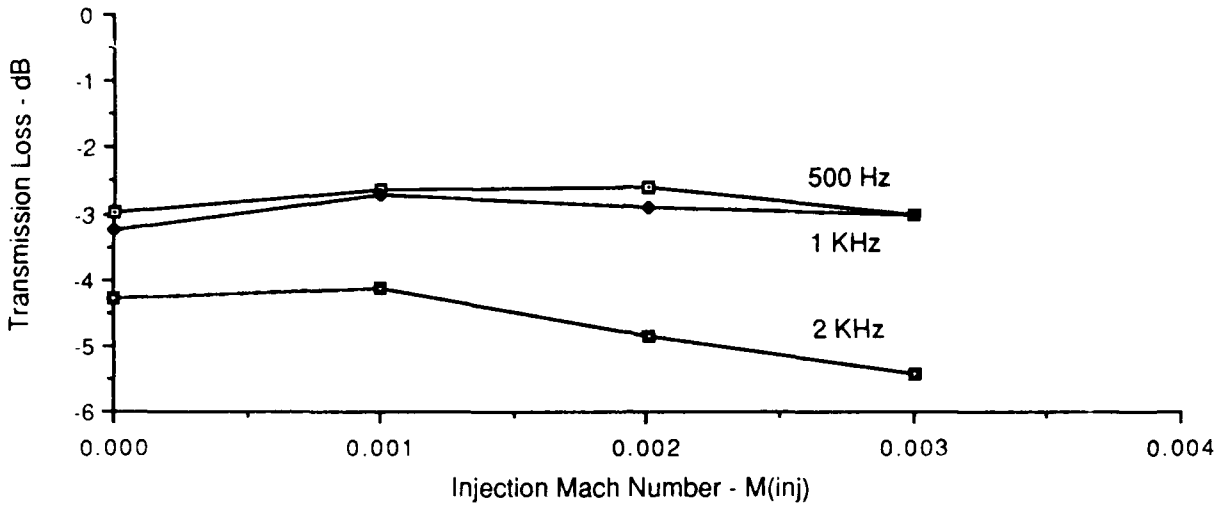

Figure 23. Measured Acoustic Transmission Loss

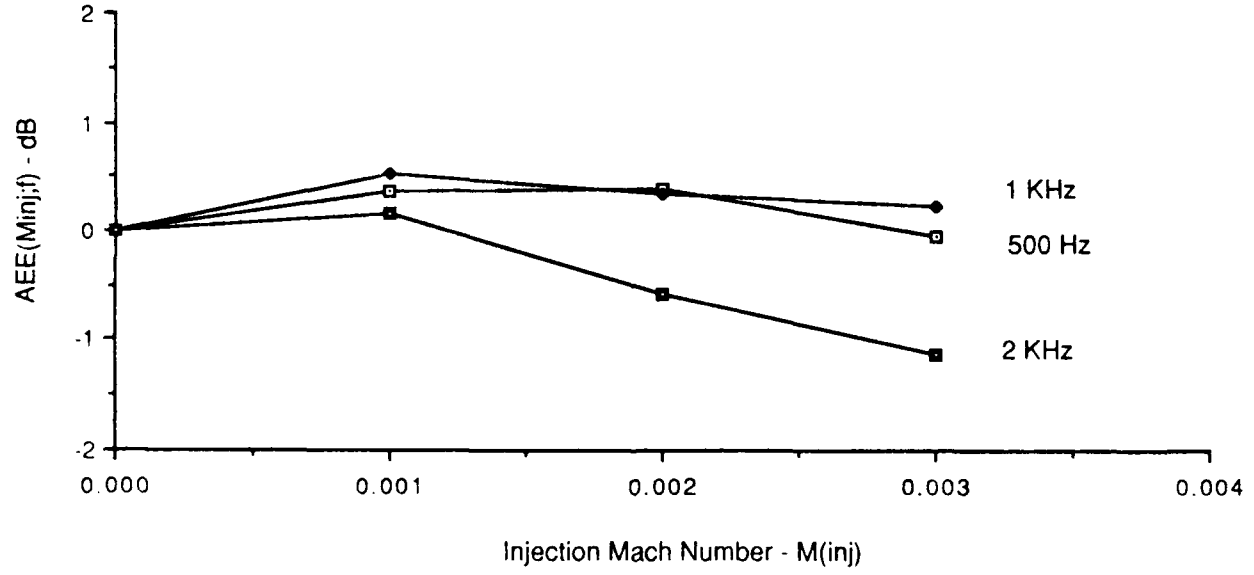

Figure 24. Measured Acoustic Energy Exchange

Several important assumptions were introduced into the model to simplify its derivation. *First,* the channel into which fluid is injected is uniform in cross-section and infinite in length. This assumption was required because Culick's model assumed that the rocket chambers were bounded by rigid walls at both ends. *Second,* longitudinal sound is assumed to be established within the channel prior to the injection of the fluid. Since the channel is infinite in length, only propagating sound waves are established within the channel. *Third,* the fluid is inviscid and non-heat conducting. *Fourth,* the temperature of the injected fluid is equal to the fluid temperature within the channel. *Fifth,* the perfect gas law is used as the equation of state of the injected fluid. And *sixth,* fluid is injected at very low volume flow rates into the channel in a uniform manner along its upper and lower walls. The fluid is injected in a direction perpendicular to the channel axis.

Derivation of Governing Acoustic Equations

A schematic of the control volume used in this derivation is shown in Figure 25. Mean flow is injected into the control volume at y = 0 and y = H as shown. Assuming the fluid is inviscid, the conservation of mass and axial momentum may be written, respectively, as

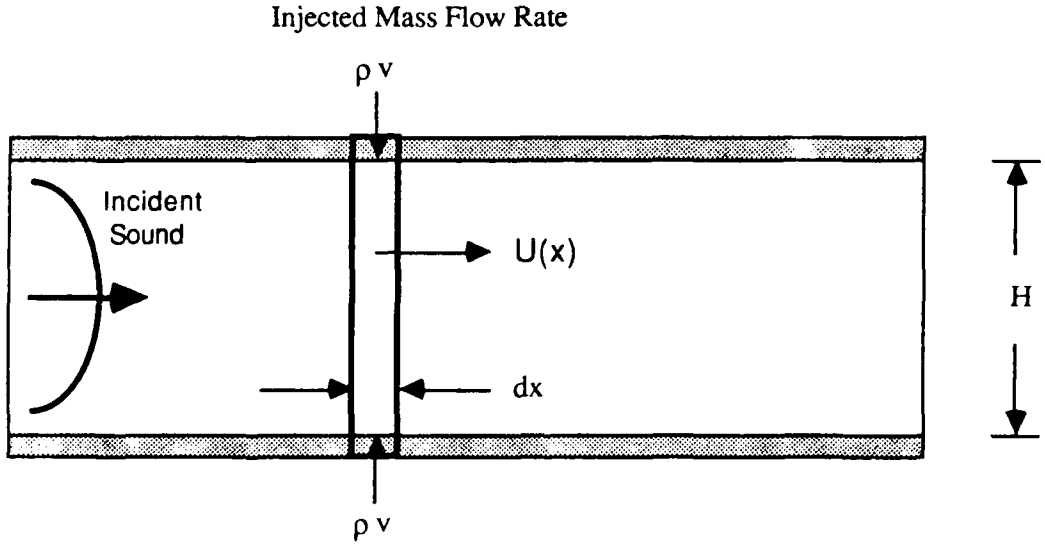

Figure 25. Control Volume Used in Model Derivation

$$\frac{\partial \rho}{\partial t} + \frac{\partial}{\partial x}(\rho u) = \frac{2}{H}\rho v \tag{11}$$

and

$$\frac{\partial u}{\partial t} + \rho u \frac{\partial u}{\partial x} + \frac{\partial p}{\partial x} = -\frac{2}{H}\rho u v \tag{12}$$

The derivation of Eq. (11) assumes that mass is pumped transverseiy, as shown schematically in Figure 25, *into* the control volume at the rate ρv per unit area. Adopting the usual practice of assuming that the instantaneous fluid properties can be decomposed into mean and acoustic components, the following conservation of acoustic mass flux is derived,

$$\frac{\partial \rho'}{\partial t} + \bar{\rho}\frac{\partial u'}{\partial x} + U\frac{\partial \rho'}{\partial x} + \frac{\partial U}{\partial x}\rho' = \frac{2}{H}(V\rho' + \bar{\rho}v') \tag{13}$$

Here (') denotes acoustic quantities and $\bar{\rho}$ denotes the constant mean fluid density. The corresponding acoustic momentum flux equation is

$$\bar{\rho}\left[\frac{\partial u'}{\partial t} + U\frac{\partial u'}{\partial x} + \frac{\partial U}{\partial x}u'\right] + \frac{\partial p'}{\partial x} = -\frac{2}{H}[\bar{\rho}Uv' + V(\bar{\rho}u' + U\rho')] \tag{14}$$

The local mean flow speed [U≡U(x)] at a distance x from the leading edge of the injection region is calculated from the conservation of volume flow. This is valid because of the very low rates at which the fluids are injected into the channel. Referring to Figure 25, the total volume flow rate injected into the channel from the upper and lower surfaces is 2xWV where V is the constant injection speed and W is the channel width. The local mean flow speed U(x) is calculated form the conservation of mean volume flow

$$2xWV = WHU(x) \quad \rightarrow \quad U(x) = 2\frac{x}{H}V \tag{15}$$

It is of interest to observe that this approach agrees exactly with the more accurate two-dimensional analysis developed by Culick[9]. The derivation of his model starts with the assumption that the injected mean flow is two-dimensional, inviscid and incompressible. The governing mean flow continuity equation is

$$\frac{\partial U}{\partial x} + \frac{\partial V}{\partial y} = 0 \qquad (16)$$

Adopting the approach used by Culick , the following solution was found,

$$U(x, y) = V_{inj}\left(\frac{\pi x}{H}\right)\sin\left(\frac{\pi y}{H}\right); \quad V(y) = V_{inj}\cos\left(\frac{\pi y}{H}\right) \qquad (17a,b)$$

The accuracy of Eq. (17a) was verified by comparing it to measured values of the mean flow profile, downstream of the injection test section where x = 16 inches. As shown in Figure 26, the agreement between prediction and measurement is excellent everywhere except near the walls where the assumption that the mean flow is inviscid is not expected to be valid. Observe that the predicted axial velocity U(x,y) satisfies the no-slip condition at the walls and that V(y) satisfies the inward injection speeds at y = 0 and y = H. Observe further that the successful prediction of the outer portion of the velocity profiles suggests that the injected mean flow streamline patterns are laminar. The average speed across the channel is calculated by substituting Eq.(17a) into Eq. (4) to yield

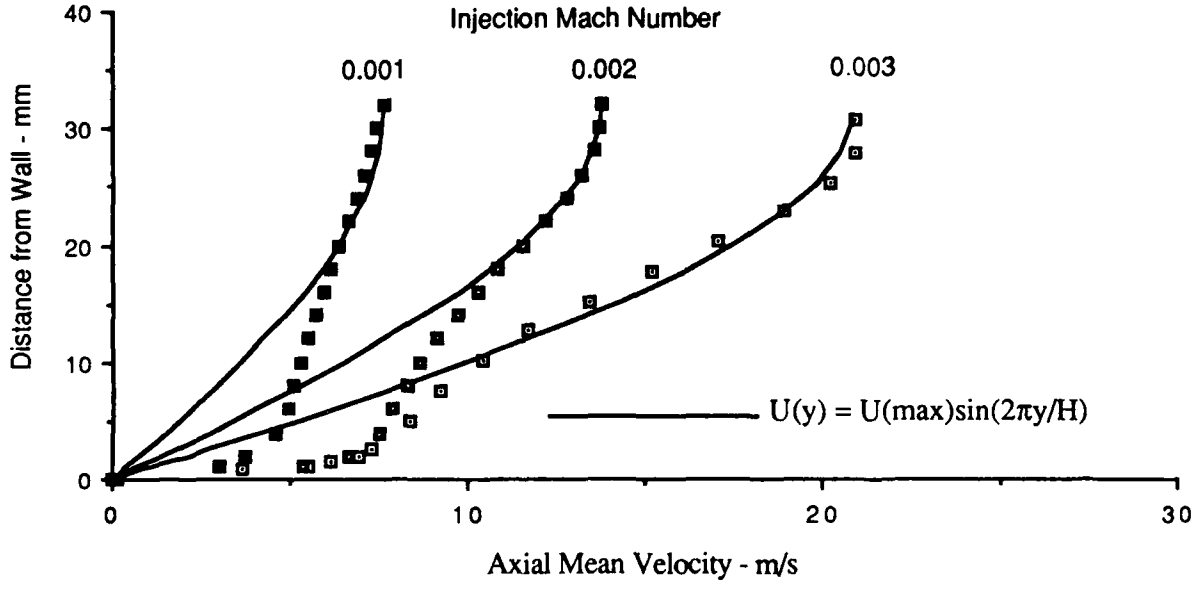

Figure 26. Plots of Predicted & Measured Velocity Profiles

$$U(x) = \frac{1}{H}\int_0^H U(x, y)\,dy = \frac{1}{H}\int_0^H \left(\frac{\pi x V}{H}\right)\sin\left(\frac{\pi y}{H}\right)dy = 2\frac{x}{H}V \qquad (18)$$

which agrees exactly with Eq. (15).

Since the fluid temperatures inside and outside of the test facility are assumed to be equal, the conservation of energy flux may be written

$$\frac{\partial}{\partial t}\left[\rho\left(e + \frac{u^2}{2}\right)\right] + \frac{\partial}{\partial x}\left(\rho u\left(e + \frac{u^2}{2}\right)\right) + \frac{\partial}{\partial x}(pu) = \frac{2}{H}\rho v\left(h + \frac{v^2}{2}\right) \qquad (19)$$

Here $e = C_V T$ is the fluid internal energy per unit mass and $h = C_p T$ is the fluid internal enthalpy per unit mass. Replacing T by the equation of state for ideal gases,

$$p = \rho RT = \frac{\rho c^2}{\gamma}; \qquad c^2 = \gamma RT \qquad (20a,b)$$

the following conservation of energy flux may be derived after some algebra,

$$\left[\frac{\partial p}{\partial t} - c^2\frac{\partial \rho}{\partial x}\right] + u\left[\frac{\partial p}{\partial t} - c^2\frac{\partial \rho}{\partial x}\right] = \frac{2}{H}\rho v\left(\frac{u^2 + v^2}{2}\right) \qquad (21)$$

Expanding Eq. (21) into mean and acoustic components and retaining terms linear in mean flow speed U yields the following acoustic conservation of energy flux,

$$\left[\frac{\partial p'}{\partial t} - c^2\frac{\partial \rho'}{\partial x}\right] + U\left[\frac{\partial p'}{\partial t} - c^2\frac{\partial \rho'}{\partial x}\right] = 0 \qquad (22)$$

Perturbation Solution

Observe that Eqs. (13, 14 & 22) contain the four unknowns, p',ρ',u' and v'. A fourth equation must be introduced in order to solve these equations. Since a one-

dimensional solution is sought, v' is connected to the sound pressure p' through the non-dimensionalized admittance of the side wall panels $A_W = A_R + iA_I$, as defined below,

$$v' = -A_w \frac{p'}{\bar{\rho}c} = -(A_R + iA_I)\frac{p'}{\bar{\rho}c} \tag{23}$$

Referring to Figure 25, in order for sound energy to be absorbed, the local acoustic velocity must be pumped *into* the walls at y = 0 and y = H. Thus v' must be negative as shown in Eq. (23). Replacing v' by Eq. (23) and substituting into Eqs. (13 & 14) yields the following equations governing the conservation of acoustic mass and axial momentum,

$$\frac{\partial \rho'}{\partial t} + \bar{\rho}\frac{\partial u'}{\partial x} = \left(\frac{2V}{H} - \frac{\partial U}{\partial x}\right)\rho' - U\frac{\partial \rho'}{\partial x} - \frac{2A_w}{cH}p' \tag{24}$$

and

$$\bar{\rho}\frac{\partial u'}{\partial t} + \frac{\partial p'}{\partial x} = \frac{2UA_w}{cH}p' - \bar{\rho}\left[\frac{2V}{H} + \frac{\partial U}{\partial x}\right]u' - \bar{\rho}U\frac{\partial u'}{\partial x} \tag{25}$$

Equations (24 & 25) can be combined into a single higher-order equation by differentiating Eq. (24) by $\partial/\partial t$ and Eq. (25) by $\partial/\partial x$ yielding

$$\frac{\partial^2 \rho'}{\partial t^2} - \frac{\partial^2 p'}{\partial x^2} + \frac{2A_w}{cH}\frac{\partial p'}{\partial t} = \frac{2V}{cH}\left\{\left[\rho c\frac{\partial u'}{\partial x} - 2\frac{A_w}{H}p'\right] + x\left[\rho c\frac{\partial^2 u'}{\partial x^2} - c\frac{\partial^2 \rho'}{\partial x \partial t} - 2\frac{A_w}{H}\frac{\partial p'}{\partial x}\right]\right\} \tag{26}$$

Equation (24) is used to eliminate u' from Eq. (26) resulting in two equations governing the time and spatial changes of p' and ρ'.

Following the approaches adopted by Culick and Flandro, approximate solutions to Eqs. (22 & 26) are sought based on the following regular power series expansion of p' and ρ' in terms of the small parameter M_{inj},

$$p'(x, t) \equiv p_0(x, t) + M_{inj}\, p_1(x, t) + M_{inj}^2\, p_2(x, t) + \ldots \tag{27}$$

and

$$\rho'(x, t) \equiv \rho_0(x, t) + M_{inj}\, \rho_1(x, t) + M_{inj}^2\, \rho_2(x, t) + \ldots \tag{28}$$

where

$$M(x) = \frac{U(x)}{c} = M_{inj}\left(\frac{2x}{H}\right); \qquad M_{inj} \equiv \frac{V}{c} \tag{29a,b}$$

Observe that the ( )' notation used to denote acoustic variables has been omitted for convenience.

Combining the resulting equations to eliminate ρ' and collecting the coefficients of the first two powers of M_{inj} leads to a collection of conservation equations modelling the behavior the sound field. For the lower-order terms (independent of M_{inj}), these equations are

$$\frac{\partial p_0}{\partial t} - c^2 \frac{\partial \rho_0}{\partial t} = 0 \tag{30}$$

and

$$\frac{\partial^2 \rho_0}{\partial t^2} - \frac{\partial^2 p_0}{\partial x^2} + \frac{2A_w}{cH}\frac{\partial p_0}{\partial t} = 0 \tag{31}$$

For the terms proportional to M_{inj}, the corresponding conservation equations are

$$\frac{\partial p_1}{\partial t} - c^2 \frac{\partial \rho_1}{\partial t} = 0 \tag{32}$$

and

$$\frac{\partial^2 \rho_1}{\partial t^2} - \frac{\partial^2 p_1}{\partial x^2} + \frac{2A_w}{cH}\frac{\partial p_1}{\partial t} =$$

$$\frac{2}{H}\left\{\left[\underbrace{3\rho c\frac{\partial u_0}{\partial x}}_{F-T} - 2\frac{A_w}{H}p_0\right] + x\left[\rho c\frac{\partial^2 u_0}{\partial x^2} - \frac{1}{c}\frac{\partial^2 \rho_0}{\partial x \partial t} - 2\frac{A_w}{H}\frac{\partial p_0}{\partial x}\right]\right\} \qquad (33)$$

The term labelled F-T in Eq. (33) represents the "flow-turning" term used in the Appendix to derive Eq. (1). This term will later be shown to dominate the behavior of the interaction between the injected fluid and the longitudinal sound field within the channel.

Equations (30 & 32) show that the acoustic pressure and density of the lowest-ordered and linear terms are adiabatically related where

$$p_0 = c^2 \rho_0 \quad \text{and} \quad p_1 = c^2 \rho_1 \qquad (34a,b)$$

Substituting Eq. (34a) into Eq. (31) yields the following lower-order wave equation governing the acoustic behavior of the sound pressure

$$\frac{1}{c^2}\frac{\partial^2 p_0}{\partial t^2} - \frac{\partial^2 p_0}{\partial x^2} + \frac{2A_w}{cH}\frac{\partial p_0}{\partial t} = 0 \qquad (35)$$

The corresponding first-order wave equation is determined by substituting Eq. (34b) into Eq. (33) to yield

$$\frac{1}{c^2}\frac{\partial^2 p_1}{\partial t^2} - \frac{\partial^2 p_1}{\partial x^2} + \frac{2A_w}{cH}\frac{\partial p_1}{\partial t} =$$

$$\frac{2}{H}\left\{\left[\underbrace{3\rho c\frac{\partial u_0}{\partial x}}_{F-T} - 2\frac{A_w}{H}p_0\right] + x\left[\rho c\frac{\partial^2 u_0}{\partial x^2} - c\frac{\partial^2 \rho_0}{\partial x \partial t} - 2\frac{A_w}{H}\frac{\partial p_0}{\partial x}\right]\right\} \qquad (36)$$

An approximate solution to Eq. (35), valid for small values of A_R and A_I, is

$$p_0(x, t) \cong C_0 e^{-A_R \frac{x}{H} + I(\omega t - kx)} \tag{37}$$

where C_0 is an arbitrary constant. Equation (37) represents an approximate solution of the sound pressure distribution within the injection test section in the absence of injection flow. Referring to the discussion following Eq. (23) , the negative sign was inserted in order to force the solution defined by Eq. (37) to agree with the measured acoustic energy transmission data (at $M_{inj} = 0$) shown in Figure 23. No attempt has been made in the above derivation to account for the effects of reflected waves. Although such a solution can be found, the algebra is very messy and little will be served. Referring to Table 1, the upstream propagating acoustic energy, which is proportional to the square of the reflection coefficient R, is quite small for all three test frequencies.

The acoustic energy transmission ratios across the test section *in the absence of injected flow* can be easily estimated from Eq. (37). Following standard acoustic analysis, the real part of the rms sound pressure is

$$p_R(x) = \frac{C_0}{\sqrt{2}} e^{-A_R \frac{x}{L}} \tag{38}$$

The acoustic energy transmission coefficient (T) across the test section follows from Eqs. (10 & 38) to be

$$T(0) \equiv 10 \text{Log}\left[\frac{p_R^2(L, 0)}{p_R^2(0, 0)}\right] = -8.69 \frac{L}{H} A_R \tag{39}$$

Equation (39) is used in conjunction with the measured T(0) data summarized in Table 2 to back-out predicted values of A_R. These values are compared to the values measured by Hersh and Walker in Figure 27. The agreement is reasonable. Since measured data was used, the values of A_R shown in Figure 27 include the effects of viscous damping.

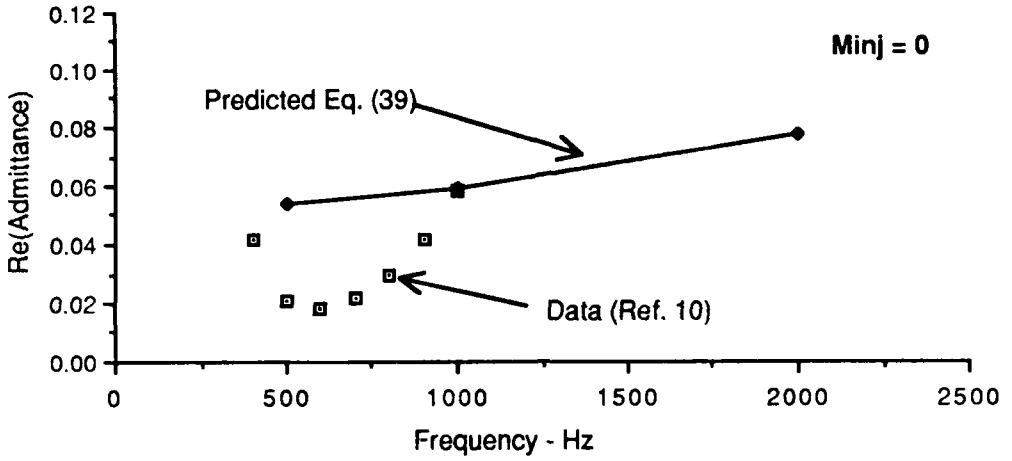

Figure 27. Predicted vs Measured Re(Admittance)

The solution to $\mathbf{p}_1$ is obtained from Eq. (36) by substituting Eq. (37) for $\mathbf{p}_0$, Eq. (34a,b) to connect p' and ρ', and using the lowest-order mass flux conservation equation to derive the following connection between the lowest-order particle velocity u_o to the pressure p_o,

$$\frac{1}{c^2}\frac{\partial p_o}{\partial x} + \bar{\rho}\frac{\partial u_o}{\partial x} = -\frac{2A_w}{cH}p_o \rightarrow \bar{\rho}\frac{\partial u_o}{\partial x} = -\frac{1}{cH}(2A_w + ikH)p_o \quad (40)$$

This yields

$$\frac{1}{c^2}\frac{\partial^2 p_1}{\partial t^2} - \frac{\partial^2 p_1}{\partial x^2} + \frac{2A_w}{cH}\frac{\partial p_1}{\partial t} =$$

$$-\frac{2p_0}{H^2}\left\{\underbrace{\left[8A_R + i(3kH + 8A_I)\right]}_{F-T} + 4\frac{x}{H}(kH + A_I)\left[(kH + 2A_I) - 2iA_R\right]\right\} \quad (41)$$

A solution to Eq. (41) is sought of the form

$$p_1'(x, y, t) = C_0 e^{-A_R \frac{x}{H} + i(\omega t - kx)} f(x) \tag{42}$$

Substituting Eqs. (37 & 42) into Eq. (41) and assuming that both $A_R \& A_I \ll 1$ leads to the following simplified differential equation governing f(x),

$$f'' - \frac{2}{H}(A_R + ikH)f' + \left(\frac{A_R}{H}\right)^2 f = \frac{1}{H^2}\{16A_R + 6ikH + 4(kx)[kH - 2iA_R]\} \tag{43}$$

Since $A_R \ll 1$, an approximate solution to Eq. (43) is sought in terms of the expansion

$$f(x) \approx f_0(x) + A_R f_1(x) + A_R^2 f_2(x) + \ldots \tag{44}$$

Substitution of Eq. (44) into Eq. (43) yields the following differential equations to order $(A_R)^2$,

$$f_0'' - 2ikf_0' = -\frac{1}{H^2}\left\{\underbrace{6ikH}_{F-T} + 4(kx)kH\right\} \tag{45}$$

$$f_1'' - 2ikf_1' = \frac{2}{H}f_0' + \frac{1}{H^2}(16 - 8ikx) \tag{46}$$

and

$$f_2'' - 2ikf_2' = \frac{2}{H}f_1' - \frac{1}{H^2}f_0 \tag{47}$$

The "flow-turning" term appears as a source term in Eq. (45). Foregoing the details, the following particular solution was derived

$$f(x) \approx \left\{ -2\frac{x}{H} + i\left[(kH)\left(\frac{x}{H}\right)^2 - \frac{1}{kH}\right]\right\} + A_R\left\{\left[\left(\frac{x}{H}\right)^2 + \frac{5}{2(kH)^2}\right] + \frac{5i}{kH}\left(\frac{x}{H}\right)\right\}$$
$$+ A_R^2\left\{\left[\frac{1}{6}\left(\frac{x}{H}\right)^3 - \frac{13}{4(kH)^2}\left(\frac{x}{H}\right)\right] + \frac{i}{4(kH)}\left[5\left(\frac{x}{H}\right)^2 + \frac{33}{2(kH)^2}\right]\right\} \quad (48)$$

The composite solution, to order M_{inj}, of the one-dimensional sound pressure distribution within the test section follows by substituting Eqs (37, 42 & 48) into Eq. (27) to yield

$$p(x, t) \cong C_0 e^{-A_R\frac{x}{H} + i(\omega t - kx)}\left[1 + M_{inj} f(x)\right] \quad (49)$$

The root-mean-square pressure distribution within the injection test section follows from application of Eq. (5) to be

$$p_R(x, M_{inj}) \cong \frac{C_0}{\sqrt{2}} e^{-A_R\frac{x}{L}}\left[1 + M_{inj} f_R(x)\right] \quad (50)$$

where

$$f_R(x) = \underbrace{-2\left(\frac{x}{H}\right)}_{F-T} + A_R\left[\left(\frac{x}{H}\right)^2 + \frac{5}{2(kH)^2}\right] + A_R^2\left(\frac{x}{H}\right)\left[\frac{1}{6}\left(\frac{x}{H}\right)^2 - \frac{13}{4(kH)^2}\right] \quad (51)$$

Here $f_R(x)$ represents the real part of f(x). The solution defined by Eq. (51) shows that the "flow-turning" contribution dominates the other terms providing AR « 1. Further, the negative sign indicates that sound energy is absorbed. Since we are dealing only with travelling waves, the acoustic energy transmission across the test section is expressed as

$$T(M_{inj}) \equiv 10Log\left[\frac{p_R^2(L, M_{inj})}{p_R^2(0, M_{inj})}(1 + M_{AV})\right] \tag{52}$$

Substituting Eq. (51) into Eq. (50) yields the following expression for the acoustic energy transmission across the test section,

$$T(M_{inj}) \cong T(0) + 10Log(1 + M_{av}) + 10Log\left[\frac{1 + M_{inj} f_R(L)}{1 + M_{inj} f_R(0)}\right] \tag{53}$$

Rewriting Eq. (53) using Eq. (2) results in the following theoretical estimate of the acoustic energy exchange (AEE) between transversely injected flow and longitudinal sound,

$$AEE \cong 10Log(1 + M_{av}) + 10Log \left\{ \frac{1 - M_{inj}\left\langle \underbrace{2\left(\frac{L}{H}\right)}_{F-T} - A_R\left[\left(\frac{L}{H}\right)^2 + \frac{5}{2(kH)^2}\right] - A_R^2\left(\frac{L}{H}\right)\left[\frac{1}{6}\left(\frac{L}{H}\right)^2 - \frac{13}{4(kH)^2}\right]\right\rangle}{1 + \frac{5A_R M_{inj}}{2(kH)^2}} \right\} \tag{54}$$

Equation (54) is the desired result. Its interpretation requires considerable comment. To begin with, observe that since AR « 1, Eq. (54) is dominated by the "flow-turning" term -2(L/H)Minj. This term can be traced to Culick's "flow-turning" loss expression defined by Eq. (1) for the special case of *rigid walls* where A_R =0. Under this condition, Eq. (54) simplifies to

$$AEE \cong 10Log(1 + M_{av}) + 10Log\left[1 - \underbrace{2M_{inj}\left(\frac{L}{H}\right)}_{F-T}\right] \tag{55}$$

Combining Eqs. (15 & 29a), the "flow-turning" term $2M_{inj}(L/H)$ in Equation (55) can be simplified by observing that

$$M_{av} \equiv 2\left(\frac{L}{H}\right)M_{inj} \tag{56}$$

Now substituting Eq. (56) into Eq.(55) produces the interesting result that

$$AEE \cong 10Log\left(1 + \underbrace{M_{av}}_{Convection}\right) + 10Log\left(1 - \underbrace{M_{AV}}_{F-T}\right) = 10Log\left(1 - M_{AV}^2\right) \tag{57}$$

Equation (57) suggests that within the context of Culick's "flow-turning" model, the interaction between the injected flow and longitudinal sound is *stabilizing* in the sense that acoustic energy is *absorbed* across the injection region. Unfortunately, the one-dimensional model is not capable of providing insight into the details of the absorption process. It is of interest to point out that the "flow-turning" losses are almost equal to the increase in acoustic energy due to the mean flow. That is, the sum of the "flow-turning" losses and the convection gains almost cancel with the resulting absorption of order $Minj^2$. It is important to understand that in rocket motor stability calculations, the convective gain in acoustic energy really represents an acoustic energy loss because the acoustic energy is convected out of the the rocket interior. The important point to be made here is that the "flow-turning" losses are of the same order-of -magnitude as the convective losses.

Equation. (57) also shows that the "flow-turning" sound absorption is independent of the sound frequency. This is what one would expect in a one-dimensional rigid wall analysis. These findings are in agreement with the 500 Hz and 1 KHz data presented in Figures 23 & 24. The effects of both injection Mach number and sound frequency were found to be negligible. This behavior is not true, however, for the 2 KHz data. Here, the amount of sound energy that is absorbed increases almost linearly with M_{inj} providing $M_{inj} > 0.1$. The data suggests that the sound absorption behavior may be controlled by the local wall admittance. Referring to Figure 27, it may be no coincidence that the values of the real part of the wall admittance are almost equal at 500 Hz ($A_R \approx 0.54$) and 1 KHz ($A_R \approx 0.59$) while the corresponding value at 2 KHz is much higher ($A_R \approx 0.77$).

Now consider what happens for finite admittance side walls. Referring to Eq. (54), the one-dimensional model predicts that the interaction between transversely injected flow and longitudinal sound results in a net *gain* of sound energy. Inserting the values of A_R displayed in Figure 27 into Eq. (54), the predicted predicted values are compared to measured data in Figure 28. The predicted gains of energy are sufficiently small that the effects of frequency variation can not be seen - they all collapse into the single curve shown. This slight increase is caused by the finite values of A_R. *It is clear that the one-*

dimensional model summarized by Eq. (54) does not agree with the data displayed in Figure 28.

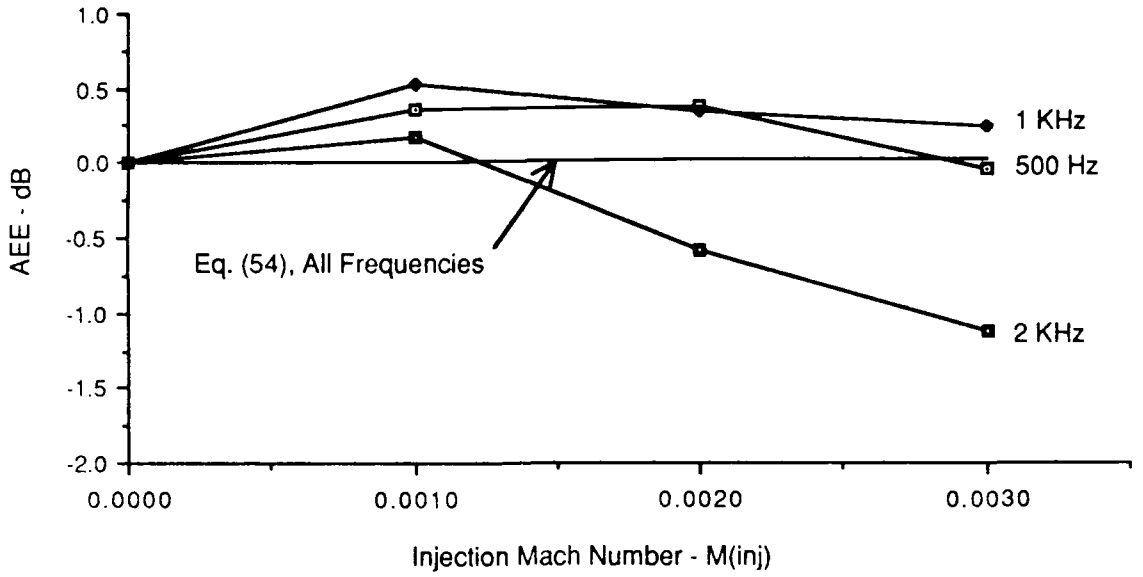

Figure 28. Comparison Between Predicted and Measured AEE

The reader is reminded that Eq. (54) is valid only for travelling waves. However, this restriction is not particularly severe because most of the sound energy is propagating downstream. This is evident from the measured small values of reflection coefficients R displayed in Table 2. Recall that R^2 is a measure of the relative fraction of the sound energy propagating upstream.

Transient Solution

Equations (35 & 36) represent the wave equations governing the behavior of the sound field within the injection test section. Transient solutions to these equations are sought in order to compare them directly to Culick's solution defined by Eq. (1). Starting with Eq. (35), the solution to the lowest order or unperturbed (i.e., $M_{inj} = 0$) wave equation is sought having the form

$$p_0(x, t) = C_0 e^{i[\omega(1 + i\alpha)t - kx]} = \underbrace{C_0 e^{-\alpha t}}_{A(t)} e^{i[\omega t - kx]} \qquad (58)$$

Equation (58) has been written to show explicitly how the amplitudes A(t) of the travelling waves decay in time for $\alpha > 0$. Substituting Eq. (58) into Eq. (35) yields the following approximate solution

$$p_0(x,t) \cong C_0 e^{-\frac{A_R ct}{H} + i[\omega t - kx]} \tag{59}$$

The decay constant α is proportional to the real part of the wall admittance A_R. This is reasonable because the transient solution defined by Eq. (59) follows immediately from the acoustic steady-state solution defined by Eq. (37) provided x and t are connected using the phase speed c of the travelling wave as shown below

$$c = \frac{dx}{dt} \quad \rightarrow \quad x = ct \tag{60}$$

The solution defined by Eqs. (59 & 60) assumes that the loss of sound energy at the wall is sufficiently weak that the sound wave can still be characterized as plane-wave. This is consistent with small values of A_R. A simple connection exists between the steady-state solution defined by Eq. (37) and the transient solution defined by Eq. (59). Equation (37) estimates the spatial decay of the amplitude of the sound wave at a fixed moment in time, while Eq. (59) estimates the time dependent decay of the amplitude of the sound wave at a fixed position in space. Assuming representative cold flow test values for the parameters governing α of c = 34,400 cm/sec, H = 6.35 cm and A_R = 0.07 yields α = 379/sec^{-1}. Finally, if the wall is rigid, then A_R = 0. and no energy is absorbed. This recovers the idealized case of plane-wave sound propagation in an infinite constant area duct.

The next step is to apply the above ideas to seek transient solutions to Eq. (36), the wave equation perturbed by the injected flow. According to Culick's model, even if the walls are rigid, sound energy should be absorbed by the turning of the injected flow. To explore this, $A_w = 0$ on the RHS of Eq. (36), leading to the simplified wave equation,

$$\frac{1}{c^2}\frac{\partial^2 p_1}{\partial t^2} - \frac{\partial^2 p_1}{\partial x^2} = \frac{2}{H}\left[\underbrace{3\rho c \frac{\partial u_0}{\partial x}}_{F-T} + x\left(\rho c \frac{\partial^2 u_0}{\partial x^2} - \frac{1}{c}\frac{\partial^2 \rho_0}{\partial x \partial t}\right)\right] \tag{61}$$
$$= -\frac{2k}{H}(3i + 2kx)$$

In deriving Eq. (61), the unperturbed acoustic velocity u_o was connected to the acoustic pressure p_o via the acoustic momentum conservation equation.

A solution to Eq. (61) is sought of the form

$$p_1(x, t) = [f(t) + xg(t)]C_o e^{i(\omega t - kx)} \tag{62}$$

Substituting Eq. (62) into Eq. (61), the real part of the solution is

$$p_1(x, t) = -\left(\frac{ct}{H} + \frac{x}{H}\right)C_o e^{i(\omega t - kx)} \tag{63}$$

The composite solution, to order M_{inj}, follows by inserting the solutions defined by Eqs. (59 & 63) into Eq. (27) to yield

$$\begin{aligned} p(x, t) &\cong \left[1 - M_{inj}\left(\frac{ct}{H} + \frac{x}{H}\right)\right]C_o e^{i(\omega t - kx)} \\ &\cong \left[1 - \left(\frac{v_b t}{H} + M_{inj}\frac{x}{H}\right)\right]C_o e^{i(\omega t - kx)} \end{aligned} \tag{64}$$

In deriving Eq. (64), k was replaced by ω/c, and cM_{inj} by v_b where v_b is Culick's expression for the rate of fluid injection at the surface.

A discussion of the meaning of Eq. (64) will be deferred until Culick's "flow-turning" estimate defined by Eq. (1) is reviewed. Referring to the derivation presented in the Appendix, p_0 represents the unperturbed pressure. For travelling wave sound propagation in rigid-walled constant area ducts, p_0 is defined as

$$p_0 = C_o e^{i(\omega t - k_1 x)} \tag{65}$$

where $k_1 = \omega/c$ using Culick's notation. Setting the constant Co = 1 without loss of generality, and substituting Eq. (65) into Eq. (1) yields the following estimate of α_{FT}

$$\alpha_{FT} = -\underbrace{\frac{q}{S_c}}_{\frac{2}{H}}\underbrace{\frac{m_b}{\bar{\rho}}}_{v_b}\frac{1}{E_l^2}\left[\underbrace{\int_0^L p_0^2 dx}_{\xi_l^2}\right] = -\frac{2v_b}{H} \tag{66}$$

The "flow-turning" decay constant defined by Eq. (66) represents a loss of energy characterized by the expression

$$p(x,\ t) = C_0 e^{-2\frac{v_b t}{H} + i(\omega t - kx)} \tag{67}$$

The acoustic energy loss in Eq. (67) is exponential. Now compare Eq. (67) to the corresponding energy loss expression defined by Eq. (64). If one assumes that $M_{inj} \ll 1$, then the term

$$\left[1 - \left(\frac{v_b t}{H} + M_{inj}\frac{x}{H}\right)\right] \cong e^{-\left(\frac{v_b t}{H} + M_{inj}\frac{x}{H}\right)} \tag{68}$$

Using Eq. (68), Eq. (64) may be approximated by the expression

$$\begin{aligned} p(x,t) &\cong \left[1 - \left(\frac{v_b t}{H} + M_{inj}\frac{x}{H}\right)\right] C_0 e^{i(\omega t - kx)} \\ &\cong C_0 e^{-\left(\frac{v_b t}{H} + M_{inj}\frac{x}{H}\right) + i(\omega t - kx)} \end{aligned} \tag{69}$$

A comparison between Eq. (67) and Eq. (69) verifies Culick's model providing the approximation defined by Eq. (68) is valid. This is important. The implication here is that if enough terms were solved for in the regular perturbation solution defined by Eq. (27), then their sum would equate to the exponential expression derived by Culick. It is clear that this is a time consuming and laborious task. This is a dramatic way of illustrating the cleverness of Culick's approach wherein he sought solutions only for the perturbed wavenumbers and not for the perturbed pressures; a far easier task.

It is of interest to compare the relative importance between the "flow-turning" time decay constant defined by Eq. (69) and the finite admittance wall absorption time decay constant defined by Eq. (59). The ratio of the decay constants are

$$\frac{\alpha_{FT}}{\alpha_{A_w}} = \frac{\frac{V_b}{H}}{\frac{A_R c}{H}} = \frac{M_{inj}}{A_R} \tag{70}$$

Substitution of representative test values, $M_{inj} = 0.003$ and $A_R = 0.07$, into Eq. (70) yields

$$\frac{\alpha_{FT}}{\alpha_{A_w}} \cong 0.04 \tag{71}$$

Equation (71) shows that even at the highest injection flow rate tested, the sound energy losses due to "flow-turning" are much smaller than the sound energy absorbed by the finite admittance side walls. Using the above parameters as an example, $\alpha_{FT} = 16$ sec^{-1} and $\alpha_{Aw} = 379$ sec^{-1}. Both the data summarized in Figures 23 & 24 and the above analysis show that the "flow-turning" losses are much smaller than the losses due to the finite admittance side walls.

CONCLUDING REMARKS

Test results show that acoustic energy is absorbed by the transverse injection of ambient air into an acoustically energized duct. The data can be partitioned into low and high frequency behaviors. For frequencies below 1 KHz, the energy absorption was negligible and independent of frequency and injection flow rate. At 2 KHz, just below the first transverse cut-on mode of the duct, over 1 dB of sound was absorbed - a significant amount - at an injection Mach number rate of 0.003. In all test cases, the sound absorbed by the finite admittance side-walls was significantly larger than that absorbed by the injected flow.

The effects of refraction of the sound pressure by the mean flow velocity gradients were found to be negligible. This was not surprising in light of the very small injection flow rates used in these tests.

One-dimensional steady-state and transient "flow-turning" solutions were derived. For the special case of rigid walls and low injection rates, the steady-state solutions showed that the "flow-turning" losses were approximately equal to $10Log(1-M_{av})$. These losses were almost cancelled by the convected energy gains which were equal to $10Log(1+M_{av})$. The contribution of the finite admittance side walls resulted in overall very small acoustic energy gains. The one-dimensional solutions inadequately predicted the measured acoustic energy losses.

The transient solution compared very favorably with Culick's model. Both estimated almost the same decay constants. Using the data as input, the models showed that the decay constants associated with the absorption of sound by the injected flow were much smaller than the decay constants associated with the absorption of sound by the finite admittance side walls. These findings cannot be blindly used to infer that "flow-turning" losses are unimportant in rocket motor applications. They are valid only for the cold flow test conditions of the facility. For example, the values of the wall admittance within rocket motors are generally much smaller than the admittance of the Glasstrate material used in this test program. An order-of-magnitude estimate of typical solid rocket admittance values can be determined from response function measurements. The response function and the wall admittance are connected as shown below,

$$R \equiv \frac{\frac{m'}{\overline{m}}}{\frac{p'}{\overline{p}}} = \frac{1}{\gamma}\left(\frac{A_w}{M_{inj}} - 1\right) \tag{72}$$

According to Dr. R. S. Brown[12], a typical value of R is about 2. Combining this with $M_{inj} = 0.003$ leads to $A_w \cong 0.006$ which is an order-of-magnitude less than the Glasstrate admittance values. Substituting these values into Eq. (70) yields the following estimate of the importance of Culick's "flow-turning" losses relative to the losses generated by liner walls within solid rocket motors ,

$$\frac{\alpha_{FT}}{\alpha_{A_w}} = 1.5 \approx O(1) \tag{73}$$

It was shown in Section 4.2 that the one-dimensional model was inadequate in predicting the measured acoustic energy losses across the injection test section. Referring to Eqs. (66 or 69), the one-dimensional model shows the "flow-turning" losses to be inversely proportional to the duct height H. This makes sense because H is the only relevant length scale available. Two (or three) - dimensional models may show that the

relevant length scale over which most of the "flow-turning" losses occur may be significantly less than H. The idea here is that near the head end, the flow penetrates efficiently into the rocket center. Near the exhaust end, however, the penetration is less efficient. This suggests an overall effective length scale less than H. If this proves to be true, then H in Eqs. (66 or 69) would be replaced with a smaller term resulting in an enhancement of the contribution of the "flow-turning" losses to the stability of solid rocket motors. The poor agreement between predicted and measured acoustic energy losses underscores the need to develop more accurate models of the acoustic energy losses associated with the injection of combustion products into the interior of solid rocket motors.

One of the important findings of this investigation is that it clearly illustrates the difficulty of using cold flow laboratory facilities to measure "flow-turning" losses. Most of the sound absorption takes place at the finite admittance side walls through which the mean flow is injected. Experimentally, this translates into trying to accurately measure small "flow-turning" losses as the differences between two relatively large terms. One needs to think of clever ways to get around this problem.

REFERENCES

1. Culick, F.E.C., "The Stability of One-Dimensional Motions in a Rocket Motor", Combustion Science. and Technology, Vol. 7, pp. 93-97, 1977.

2. Culick, F.E.C., "Stability of Three-Dimensional Motions in a Combustion Chamber", Combustion Science. and Technology, Vol. 10, pp. 109, 1975.

3. Culick, F.E.C., "Remarks on Entropy Production in the One-Dimensional Approximation to Unsteady Flow in Combustion Chambers", Combustion Science. and Technology, Vol. 15, pp. 93, 1977.

4. Culick, F.E.C., Magiawala, K., Wat, J., Awad, E., and Kubota,T., Measurements of Energy Losses Associated with Interactions between Acoustic Waves and Non-Uniform Steady Flow, AFRPL-TR-81-22, July, 1981.

5. Flandro, G.A., "Solid Propellant Acoustic Admittance Corrections", Journal of Sound and Vibration, Vol. 36, No. 3, 1974, pp. 297-312.

6. Vuillot, F. and Kuentzmann, P., "Flow Turning and Admittance Correction: An Experimental Comparison", Journal of Propulsion and Power, Vol. 2, No. 4, July-August 1986, pp. 345-353.

7. Baum, J.D. and Levine, J.N., Acoustic-Mean Flow Interaction, AFRPL TR-86-065, January, 1987.

8. Van Moorhem, W. K. ,"Theoretical Basis of the Flow Turning Effect in Combustion Stability", UTEC ME 80-033, Univ. of Utah, Salt Lake City, Utah., March, 1980.

9. Culick, F. E. C., "Rotational Axisymmetric Mean Flow and Damping of Acoustic Waves in a Solid propellant Rocket", AIAA Journal, Vol 4, No. 8, August, 1966, pp. 1462-1464.

10. Hersh, A. S. and Walker, B., Experimental Investigation of Rocket Motor Flow-Turning Acoustic Losses, AFRPL TR-84-009, May, 1984.

11. Pridmore-Brown, D.C., "Sound Propagation in a Fluid Flowing Through an Attenuating Duct", J. Fluid Mech., Vol.4, pp. 1393, 1958.

12. Brown, R. S., Telephone communication concerning solid rocket response functions, Sr. Scientist, United Technologies Chemical Systems, San Jose, CA., 12 January, 1988.

APPENDIX - DERIVATION OF FLOW TURNING LOSSES

For the convenience of the reader, a detailed derivation of Eq. (1) is derived below in order to understand what is meant by the term "flow-turning" losses. The derivation is based in part upon the earlier work of Culick, et. al[4]. Consider the control volume sketched below consisting of the transverse injection of flow into a uniform channel of height H with no combustion,

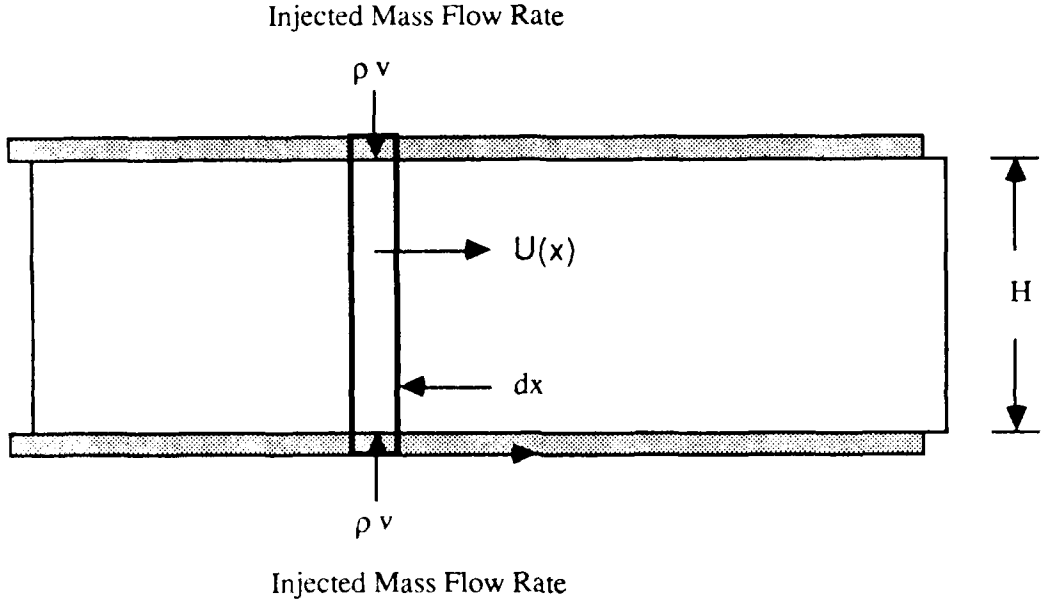

Figure A-1. Control Volume Used in Model Derivation

The injected flow is assumed to be inviscid. Restricting the flow within the channel to be one-dimensional, the conservation equations of mass and momentum flux can be written

$$\frac{\partial \rho}{\partial t} + \frac{\partial}{\partial x}(\rho u) = \frac{2}{H}\rho v \qquad \text{(A-1)}$$

and

$$\frac{\partial u}{\partial t} + \rho u \frac{\partial u}{\partial x} + \frac{\partial p}{\partial x} = -\frac{2}{H}\rho u v \qquad \text{(A-2)}$$

The derivation of the above equations assumes that mass is transversely pumped *into* the control volume at the rate ρv per unit area. The usual practice is assumed that the instantaneous fluid properties can be decomposed into mean and acoustic components,

$$\rho = \bar{\rho} + \rho'; \ \mathbf{p} = \bar{\mathbf{p}} + \mathbf{p}'; \ \mathbf{u} = \mathbf{U}(\mathbf{x}) + \mathbf{u}'; \quad \mathbf{v} = \mathbf{V} + \mathbf{v}' \tag{A-3}$$

The mean velocities U & V are connected via the steady-state conservation of mass flux equation. Inserting Eq. (A-3) into Eqs. (A-1 & A-2) yields the following conservation of acoustic mass and momentum flux equations,

$$\frac{\partial \rho'}{\partial t} + \bar{\rho}\frac{\partial \mathbf{u}'}{\partial \mathbf{x}} = \frac{2}{\mathbf{H}}(\mathbf{V}\rho' + \bar{\rho}\mathbf{v}') - \mathbf{U}\frac{\partial \rho'}{\partial \mathbf{x}} + \frac{\partial \mathbf{U}}{\partial \mathbf{x}}\rho' \tag{A-4}$$

and

$$\bar{\rho}\frac{\partial u'}{\partial t} + \frac{\partial p'}{\partial x} = -\frac{2}{H}\left[\bar{\rho}Uv' + V\left(\underbrace{\bar{\rho}u'}_{F-T} + U\rho'\right)\right] - \bar{\rho}U\frac{\partial u'}{\partial x} - \bar{\rho}\frac{\partial U}{\partial x}u' \tag{A-5}$$

The RHS of Eqs. (A-4 & A-5) contain five terms which were generated from the injected flow. Culick observes that the RHS terms may be considered to be source terms for the LHS by expanding the acoustic pressure, density and particle velocity in powers of V, the mean injection speed. With regard to deriving the "flow-turning" losses identified as Eq. (1) in the Introduction, the only (source) term to be retained is the one identified within the brackets on the RHS of Eq. (A-5). The resulting simplified equations are

$$\frac{\partial \rho'}{\partial t} + \bar{\rho}\frac{\partial \mathbf{u}'}{\partial \mathbf{x}} = \mathbf{0} \tag{A-6}$$

for the continuity flux equation and

$$\bar{\rho}\frac{\partial \mathbf{u}'}{\partial t} + \frac{\partial \mathbf{p}'}{\partial \mathbf{x}} = -\frac{2}{\mathbf{H}}\bar{\rho}\mathbf{V}\mathbf{u}' \tag{A-7}$$

for the momentum flux equation. Observe from comparing Eqs. (A-6 & A-7) with Eqs. (A-4 & A-5) that the "flow-turning" losses represent only one of many acoustic sources. The relative importance of this source is compared to the others in Section 4.

Since no combustion is assumed to be taking place and the rate at which air is injected into the channel is very low, fluctuations of the fluid pressure and density take place adiabatically and the acoustic energy flux conservation equation may be written

$$p' = c^2 \rho' \tag{A-8}$$

where c is the fluid speed of sound. The wave equation is derived in the usual way by using Eq. (A-8) to eliminate ρ' and differentiating Eq. (A-6) with respect to time and Eq. (A-7) with respect to distance to yield

$$\frac{\partial^2 p'}{\partial x^2} - \frac{1}{c^2}\frac{\partial^2 p'}{\partial t^2} = -\frac{2}{H}\bar{\rho} V \frac{\partial u'}{\partial x} \tag{A-9}$$

In the absence of injected flow, Eq. (A-9) reduces to the familiar wave equation,

$$\frac{\partial^2 p'_0}{\partial x^2} - \frac{1}{c^2}\frac{\partial^2 p'_0}{\partial t^2} = 0 \tag{A-10}$$

where p'_0 denotes that the sound pressure is unperturbed by the injected flow.

The boundary conditions associated with Eqs. (A-9 & A-10) require special comment. Culick assumes the constant area channel is bounded by end walls at x = 0,L. The unperturbed acoustic particle velocities at these locations vanish. Applying these boundary conditions to the unperturbed and perturbed wave equations, yields, respectively

$$\frac{\partial p'_0}{\partial x} = 0 \qquad (x = 0,\ L) \tag{A-11}$$

and

$$\frac{\partial p'}{\partial x} = -\frac{2\bar{\rho}Vu'}{H}, \qquad (x = 0,\ L) \tag{A-12}$$

The boundary conditions specified by Eq. (A-12) are not clear. We presume that Culick allows the small amount of volume flow generated within the channel to "somehow" leak through the end walls at x = 0 and x =L; otherwise u' vanishes.

The wave equations defined by Eqs. (A-9 & A-10) are simplified by assuming the standard time dependence

$$\mathbf{p'(x,\,t) = e^{i\omega t}p(x);} \qquad \mathbf{u'(x,\,t) = e^{i\omega t}u(x)} \tag{A-13}$$

Substituting Eq. (A-13) into Eqs. (A-9 & A-10) results in the following simplified expressions,

$$\frac{d^2 p}{dx^2} + k^2 p = -\frac{2}{H}\bar{\rho}V\frac{du}{dx} \tag{A-14}$$

and

$$\frac{d^2 p_0}{dx^2} + k_1^2\, p_0 = 0 \tag{A-15}$$

Culick used a rather clever scheme to derive Eq. (1) of the Introduction. To begin with, he multiplied Eq. (A-14) by p_0 and Eq. (A-13) by p, subtracted one from the other and integrated over the length L of the channel to yield

$$\int_0^L \left[p_0 \frac{d^2 p}{dx^2} - p\frac{d^2 p_0}{dx^2} \right] dx + \left(k^2 - k_1^2\right) \int_0^L p p_0\, dx = -\int_0^L \left[\frac{d}{dx}\left(\frac{2}{H}\rho V u\right) \right] p_0 dx \tag{A-16}$$

Integrating the first by parts and applying the boundary conditions defined by Eqs. (A-11 & A-12) produces the following expression for k^2,

$$k^2 = k_0^2 + \frac{1}{E_1^2}\int_0^L \left(\frac{2}{H}\bar{\rho}Vu\right)\frac{dp_0}{dx}dx \tag{A-17}$$

where

$$E_1^2 = \int_0^L pp_0 dx \approx \int_0^L p_0^2 dx \tag{A-18}$$

Now Eqs (A-7 & A-13) connect the velocity u to the pressure p. To lowest-order,

$$i\bar{\rho}\omega u = -\frac{dp}{dx} \tag{A-19}$$

Substituting Eq. (A-19) into Eq. (A-18) yields

$$k^2 - k_1^2 = \frac{2i}{HE_1^2}\int\left(\frac{\bar{\rho}v_b}{\bar{\rho}ck_1}\right)\left(\frac{dp_0}{dx}\right)^2 dx \tag{A-20}$$

The LHS of Eq. (A-17) can be approximated by the expression

$$k^2 - k_1^2 = \left(\frac{\omega - i\alpha}{c}\right)^2 - k_1^2 \cong k_1^2 - 2ik_1\frac{\alpha}{c} - k_1^2 = -2ik_1\frac{\alpha}{c} \tag{A-21}$$

The derivation closes by combining Eqs. (A-21 & A-20) yielding the desired result

$$\alpha_{FT} = -\frac{1}{HE_1^2}\int\left(\frac{m_b}{\rho}\right)\left(\frac{1}{k_1^2}\frac{dp_0}{dx}\right)^2 dx \tag{A-22}$$

Referring to (Eq. 1) in the Introduction, the quantity q represents the perimeter over which fluid is injected into the channel interior of cross-section S_c. Referring to Figure A-1, q = 2W where W is the width of the channel. The channel cross-section area S_c = WH. Thus $q/S_c = 2/H$. Finally, the quantity $m_b = \rho V$. With these understandings, Eqs (1 & A-22) are equivalent.

END

5-89

DTIC